NASA Contractor Report 172474

NASA-CR-172474
19850002930

DEFORMATIONS AND STRAINS IN ADHESIVE JOINTS BY MOIRE INTERFEROMETRY

Daniel Post, Robert Czarnek, Judy Wood,
Duksung Joh, and Steven Lubowinski

VIRGINIA POLYTECHNIC INSTITUTE
AND STATE UNIVERSITY
Blacksburg, Virginia

Grant NAG1-227
October 1984

National Aeronautics and
Space Administration

Langley Research Center
Hampton, Virginia 23665

11 1 1 RN/NASA-CR-172474

DISPLAY 11/2/1

85N11238*# ISSUE 2 PAGE 185 CATEGORY 27 RPT#: NASA-CR-172474 NAS 1.26:172474 CNT#: NAG1-227 84/10/00 44 PAGES UNCLASSIFIED DOCUMENT

UTTL: Deformations and strains in adhesive joints by moire interferometry

AUTH: A/POST, D.; B/CZARNEK, R.; C/WOOD, J.; D/JOHN, D.; E/LUBOWINSKI, S.

CORP: Virginia Polytechnic Inst. and State Univ., Blacksburg. CSS: (Dept. of Engineering Science and Mechanics.) AVAIL.NTIS SAP: HC A03/MF A01

MAJS: /*ADHESIVE BONDING/*DEFORMATION/*DISPLACEMENT/*LAP JOINTS

MINS: / FATIGUE (MATERIALS)/ MOIRE INTERFEROMETRY/ TIME DEPENDENCE/ VISCOELASTICITY

ABA: Author

ABS: Displacement fields in a thick adherend lap joint and a cracked lap shear specimen were measured by high sensitivity moire interferometry. Contour maps of in-plane U and V displacements were obtained across adhesive and adherent surfaces. Loading sequences ranged from modest loads to near-failure loads. Quantitative results are given for displacements and certain strains in the adhesive and along the adhesive/adherend boundary lines. The results show nonlinear displacements and strains as a function of loads or stresses and they show viscoelastic or time-dependent response. Moire interferometry is an excellent method for experimental studies of adhesive joint performance. Subwavelength displacement resolution of a few micro-inches, and spatial resolution corresponding to 1600 fringes/inch (64 fringes/mm), were obtained in these studies. The

ENTER

TABLE OF CONTENTS

ABSTRACT

Displacement fields in a thick adherend lap joint and a cracked lap shear specimen were measured by high-sensitivity moire interferometry. Contour maps of in-plane U and V displacements were obtained across adhesive and adherend surfaces. Loading sequences ranged from modest loads to near-failure loads. Quantitative results are given for displacements and certain strains in the adhesive and along the adhesive/adherend boundary lines. The results show non-linear displacements and strains as a function of loads or stresses; and they show viscoelastic or time-dependent response.

Moire interferometry is an excellent method for experimental studies of adhesive joint performance. Subwavelength displacement resolution of a few micro-inches, and spatial resolution corresponding to 1600 fringes/inch (64 fringes/mm), were obtained in these studies. The whole-field contour maps offer insights not available from local measurements made by high-sensitivity gages.

KEY WORDS

adhesive joints

thick adherend lap joint

cracked lap shear specimen

moire interferometry

experimental analysis

displacement fields

strains

INTRODUCTION

Experimental analysis of deformations in adhesively bonded joints was undertaken. Two geometries were investigated -- the thick adherend lap joint and the cracked lap shear specimen specified in Fig. 1 -- with aluminum adherends and epoxy adhesive. Deformations were recorded at several load levels, up to nearly the failure loads.

A relatively new experimental method was used: high sensitivity moire interferometry. High sensitivity moire interferometry is an optical method that yields whole-field contour maps (or fringe patterns) of in-plane displacement components, U and V. Sensitivity is 16.4 μin. per fringe order (0.417 μm/fringe order), which is in the subwavelength range. Diffraction gratings of 30,460 lines per inch (1200 ℓ/mm) are replicated on the specimen and interrogated by a reference grating of 60,960 ℓ/in. (2400 ℓ/mm). Sensitivity corresponds to the frequency of the reference grating.

This was an exploratory investigation to determine the applicability of moire interferometry for the analysis of adhesive joints. The specimens were provided by NASA Langley Research Center and were machined at VPI & SU to the widths shown in Fig. 1.

MOIRE INTERFEROMETRY

Moire interferometry is a whole-field optical method using coherent laser light to measure in-plane displacements. A comprehensive description appears in Ref. 1. Briefly, a high frequency crossed-line diffraction grating is replicated on the specimen surface using a special mold, as illustrated in Fig. 2a. The result is a thin -- usually 0.001 in. (0.025 mm) -- reflective phase grating firmly adhered to the specimen, which deforms together with the specimen surface. The specimen grating is observed in an optical arrangement

illustrated in Fig. 2b. Two beams of light incident at angles α and $-\alpha$ form a virtual reference grating. Its frequency is $f = (2 \sin \alpha)/\lambda$, where λ is the wavelength of the light. This reference grating interacts with the specimen grating to form the two-beam interference pattern recorded in the camera. When the reference grating lines are perpendicular to the x axis, the pattern is a contour map of displacements governed by the relationship

$$U = \frac{1}{f} N_x \tag{1}$$

where U is the in-plane x component of displacement at any point and N_x is the fringe order at that point in the fringe pattern.

In this work, the crossed-line grating was applied in the xy plane with lines perpendicular to the x and y axes. When the reference grating lines were perpendicular to the y axis, in-plane displacements V were obtained from fringe orders N_y by

$$V = \frac{1}{f} N_y \tag{2}$$

Frequency f was 60,960 lines/in. (2400 ℓ/mm). An argon ion laser was used at wavelength 20.3 μin. (0.514 μm) and 100 mW power. The optical arrangement used in these experiments had two additional mirrors (not shown) which produced a virtual reference grating perpendicular to that of Fig. 2b. Individual patterns of N_x or N_y were obtained by blocking the light of the alternate virtual reference grating.

PRELIMINARY TESTS

Thick Adherend Lap Joint

Tests were conducted to assess the deformations to be encountered and to determine the failure loads. A very stiff screw-type loading fixture was employed. It had a tension link with a four-arm strain gage bridge to measure the loads. The specimen grating was replicated with an epoxy resin, Photolastic PC-10C*, which resulted in a grating thickness of about 0.001 in. (.025 mm).

Results are shown in Fig. 3 for the longitudinal, or U, displacement field at a modest load. Figures 3b and c are enlargements that show remarkable spatial resolution; gradients as high as 1600 fringes/in. (64 fringes mm) are illustrated. The U-fringes in the adhesive remain essentially parallel to the adhesive/adherend interface right up to the end of the joint. They indicate, together with information from the V-field (not shown here, but see Fig. 4e for a similar pattern), either that the strain concentrations near the geometric discontinuity are extremely small, or else they are very highly localized. This conclusion applies to concentrations of normal and shear strains: ε_x, ε_y and γ_{xy}. Further work, beyond the scope of this research, is suggested to investigate the question of concentrations of shear and normal stresses in the adhesive, using enlarged models of the joints.

At higher loads the strain in the adhesive exceeded the strain capacity of the epoxy used to form the specimen grating. The grating separated and cracked in regions of very high strains.

* A product of Measurements Group, Inc., Raleigh, NC 27611. Neither NASA nor VPI & SU specifically endorse any commerical product reported here.

Improvements

The preliminary tests showed that a high elongation grating replication material is required, and they showed that very high fringe orders and severe fringe gradients are encountered. Subsequently, specimen gratings were replicated with Photolastic PC-6C epoxy, which has a specified elongation of 50%. Specimen grating thickness of 0.002 in. (0.05 mm) was obtained with this more viscous cement.

The severe fringe gradients were expected to exceed the resolution capability for high load levels and fringes were expected to be absent in the highly strained adhesive. Because of this, alternate paths were introduced in the thick adherend lap joint to maintain continuity of the fringe count between the two adherends. These were omega-shaped bridges seen in Figs. 4a-e. Their boundaries are marked in Fig. 4a by dashed lines. The bridges were made of PC-6C epoxy, which has a modulus of elasticity of approximately 30,000 psi (210 MPa). With their low modulus and their low-stiffness geometry, the bridges did not contribute in any significant amount to the load-bearing characteristics of the specimen.

Cracked Lap Shear Specimen

The same high-elongation epoxy was used for specimen grating replication. However, bridges were not used. Strains in the adhesive remained sufficiently low in locations away from the end of the lap to retain visibility of fringes and provide a path for a continuous fringe count between the adherends.

TEST SEQUENCE

The load (or stress) and longitudinal displacement history is shown in Fig. 5 for the thick adherend lap joint specimen. The corresponding history for the cracked lap shear specimen is shown in Fig. 12. Photographs of the U-displacement fields were taken at two times for each loading level, as indicated by two points on each step.

The loading screw was adjusted at the beginning of each step and then held fixed for the duration of the step. Displacement at the loading pins remained essentially fixed for each step, while the specimen exhibited creep and the load relaxed.

RESULTS

Thick Adherend Lap Joint

Fringe patterns of N_x, or U-displacement fields, are shown in Figs. 4a-d for each load step. These are the patterns photographed 16 minutes (approximately) after each load application. Figure 4e shows the pattern of N_y, or the V displacement field, for the intermediate load step, with average shear strain, τ, of 1,990 psi (13.7 MPa). Average shear strain, τ, in the lap joint is the applied load divided by the lap area (a multiplied by b). Numbers on the patterns are fringe orders, N_x or N_y. Location of the zero-order fringe is arbitrary, because rigid body translations are unimportant for deformation analyses. For the patterns in this paper, the zero fringe datum was assigned to either the center of a light fringe or the center of a dark fringe.

The fringe count across the adhesive is clearly visible in Fig. 4a and the bridges are superfluous. Fringes in the adhesive are absent in Figs. 4b-d, however, and the fringe count is accomplished in a path through the

bridges. One bridge would be sufficient, but the second provides a reassuring check of fringe count. While fringes in the bridges are not clearly reproduced in Figs. 4c-d, they were clearly visible on the photographic film and were counted with the aid of magnification.

The absence of fringes in the adhesive in these last patterns does not mean the specimen is broken. It means only that light from the adhesive zone did not enter the camera, thus darkness prevailed in this zone.

Figure 4e shows that transverse displacements across the adhesive thickness are exceedingly small. At the center of the lap, transverse displacement in the adhesive is negative. The sign of the fringe gradient is determined by a simple test: apply a tiny force to the specimen in the positive y-direction to induce positive V displacements and observe the motion of the N_y fringes; as the specimen moves, the fringes move in the direction of decreasing fringe order.

Figure 5 illustrates the stress and displacement history for this series of tests. The peaks in the shear stress (τ) graph are calculated from real data, inasmuch as the maximum load at the beginning of each load step was measured. The corresponding displacements (ΔU_C) are unknown, because fringe photographs could not be taken at zero time after load application. Very dramatic creep and load relaxation is evident at high stress and strain levels. The adhesive is responsible for these nonlinearities because stress in the aluminum adherends is well within the elastic range.

Data for Fig. 6 is taken from the preliminary test illustrated in Fig. 3. Figure 6 is a graph of the longitudinal displacements ΔU along line CC' as a function of position y. ΔU represents the displacement U at each point, using point C as the zero displacement datum. The positions of fringes along CC' (Fig. 3b) were measured from the photographic negative by means of a

micrometer stage on a high magnification profile projector. The graph shows a linear deformation across the full thickness of the adhesive.

Let us return now to the series of tests defined in Fig. 5. Figure 7 shows the variation of longitudinal displacement ΔU across the adhesive thickness as a function of position, x, along the lap joint. The variation with x is remarkably small. Indeed, one may view the longitudinal displacement across the adhesive thickness as a constant (rigid adherends) plus a small effect afforded by the elasticity of the aluminum adherends.

While the fringes in the adhesive are not visible in the patterns of Figs. 4b-d, the fringe orders in the aluminum at the adhesive interface provided the data for these curves.

Relative displacements across the adhesive at the center of the lap are plotted in Fig. 8 as a function of average shear stress in the lap. Nonlinearity and time dependence of the adhesive are illustrated quantitatively. The dashed portion of the 1-minute curve provides an estimate, however, based upon the position of the 3-minute data point.

The transverse displacements across the adhesive, ΔV_C, are exceedingly small. The small scatter in the data attests to the high resolution capability of moire interferometry, wherein fractional fringe orders can be assessed by interpolation.

The average shear strains in the adhesive at the center of the lap (along CC') can be inferred from displacements ΔU_C, even though the strains and rotations are large. This is shown as follows. For large strains, the Lagrangian strain-displacement relationships are, for shear,

$$\gamma_{xy}^{L} = \arcsin \frac{\frac{\partial U}{\partial y} + \frac{\partial V}{\partial x} + \left(\frac{\partial U}{\partial x}\right)\left(\frac{\partial U}{\partial y}\right) + \left(\frac{\partial V}{\partial x}\right)\left(\frac{\partial V}{\partial y}\right) + \left(\frac{\partial W}{\partial x}\right)\left(\frac{\partial W}{\partial y}\right)}{(1 + \varepsilon_x^L)(1 + \varepsilon_y^L)} \qquad (3)$$

and for normal strains,

$$\varepsilon_x^L = \sqrt{1 + 2\frac{\partial U}{\partial x} + \left(\frac{\partial U}{\partial x}\right)^2 + \left(\frac{\partial V}{\partial x}\right)^2 + \left(\frac{\partial W}{\partial x}\right)^2} - 1 \tag{4a}$$

$$\varepsilon_y^L = \sqrt{1 + 2\frac{\partial V}{\partial y} + \left(\frac{\partial U}{\partial y}\right)^2 + \left(\frac{\partial V}{\partial y}\right)^2 + \left(\frac{\partial W}{\partial y}\right)^2} - 1 \tag{4b}$$

where superscript L specifies the Lagrangian description and W is the out-of-plane displacement, i.e., the displacement component in the z direction. In the present case, at the center of the lap (along line CC'), the quantities $\partial V/\partial x$, $\partial U/\partial x$ and $\partial W/\partial x$ are very small compared to $\partial U/\partial y$; in addition, ε_x and ε_y are very small compared to $\partial U/\partial y$ and compared to unity. Consequently,

$$\gamma_{xy} = \arcsin\frac{\partial U}{\partial y} \tag{3a}$$

is a good approximation of the shear strain in the adhesive at the center of the lap. The gradient $\partial U/\partial y$ is a constant (Fig. 6) and deletion of the arcsin causes an error up to only 1% for gradients up to 0.25 m/m. Therefore, the shear strain may be written

$$\gamma_{xy} = \frac{\Delta U}{\Delta y} \tag{3b}$$

where Δ signifies the change in the finite distance CC'. Here, ΔU_C across the adhesive thickness is given in Fig. 8 and Δy is the adhesive thickness, 0.0087 in. (0.22 mm). The shear strain is ΔU_C divided by a constant. The γ_{xy} scale is provided in Fig. 8 on this basis, and the curves represent average shear strain on CC' vs. shear stress.

It is tempting to convert the ΔV_c curve to strain ε_y by the small strain relationship

$$\varepsilon_y = \Delta V/\Delta y \tag{5}$$

However, the term $\partial U/\partial y$ in Eq. 4b is not negligible in this case and the simple conversion is not permissible.

Longitudinal displacements and strains on the adhesive/adherend boundary line are plotted in Fig. 9 as a function of position x along the line. The gradients of longitudinal displacements U with respect to x are obviously very much smaller than with respect to y. Longitudinal strains along the boundary line A'B'D' are plotted for one load level, (τ = 2770 psi). These were determined by graphical differentiation of the corresponding displacement curve. The accuracy of this ε_x curve is much less than that of the displacement curves, because differentiation of experimental data always results in a band of uncertainty that is much broader than the uncertainty in the data. Here, the error in ε_x at any position x is estimated to be within 15% of the peak strain, or within about 200 μm/m.

One could speculate on the values of ε_x in the adhesive on the midplane between ACB and A'C'B'. By symmetry, the curve of ε_x on ACB must be the mirror image of that shown in Fig. 9. Assume ε_x varies linearly with y across the adhesive, which is likely to be a good approximation of the truth. Then, for any value of x, the average value of ε_x taken from the curve and its mirror image is predicted as the midplane strain. This midplane curve of ε_x vs. x is shown in Fig. 10. With this assumption, ε_x is nearly constant with a value equal to that at point C, except near the ends of the joint. Near A and B, the midplane value of ε_x peaks at a higher strain -- about 25% higher -- and then drops to zero at the free boundary.

It is clear that ε_x in the adhesive is controlled by the stiff adherends. Its magnitude throughout the adhesive is small compared to shear strain γ_{xy} in the adhesive. Near point C, ε_x is more than two orders of magnitude smaller than γ_{xy}. This huge difference can be verified by comparing strains at C for equal stress levels in Figs. 8 and 9.

Cracked Lap Shear Specimen

Fringe patterns of N_x, or U-displacement fields, are shown in Figs. 11a-e for each load step. These U displacement fields were photographed 7 minutes after load application, except Fig. 11b, which was exposed 10 minutes after load application. Figure 11f shows the N_y, or V displacement field for the second load step, where average tensile stress, σ, was 25,400 psi (175 MPa) and the photograph was taken 1 minute after load application. Average tensile stress, σ, is defined as the tensile load, P, divided by the cross-sectional area (a multiplied by b) of the longer adherend.

The patterns show clearly defined fringes, except in the adhesive near the left end. These reproductions are inferior to the films and photographic prints, where much stronger fringe gradients remained visible. In every case, fringes in the adhesive at the right side of the figure were clearly resolved. They provided the continuous path for continuity of fringe counts between the two adherends.

Yielding in the lower adherend definitely occurred by the fourth load step, where σ = 51,800 psi (357 MPa), as evidenced by the waviness of fringes in the left side of Figs. 11d and e. The slight waviness below the joint discontinuity in Fig. 11c (and its absence in Fig. 11b) suggests that localized yielding had already begun by the third loading step, where the average tensile stress, σ, was 38,300 psi (264 MPa).

The photographs suggest that a crack had formed at the joint discontinuity along the lower adhesive/adherend interface by the fourth loading step (σ = 51,800 psi = 357 MPa). However, the evidence is not conclusive.

The load or stress history and the history of longitudinal displacements across the adhesive thickness on line AA' are illustrated in Fig. 12. The nonlinearities are much smaller than those for the thick adherend lap specimen. This is true even though yielding of the aluminum adherends was present in the second half of the history.

Figure 13 shows the longitudinal displacements ΔU across the adhesive thickness as a function of distance x from the joint discontinuity. The displacements attenuate gradually with x. At x = 0.5 in. (13 mm), ΔU has diminished to about 10% of its peak value. Many fringes were available for these measurements, as seen in Fig. 11a-e, which translates to results of high accuracy. The maximum error is estimated to be 1% of the peak value.

The longitudinal displacement, ΔU_A, across AA' is a nonlinear function of stress or applied load, as seen in Fig. 14. Viscoelastic material behavior is less significant here than in the thick adherend lap joint, because the spread between data taken one and seven minutes after load application is small.

Figure 15 shows the transverse displacement across the adhesive thickness as a function of distance from the joint discontinuity. The data was taken from the fringe pattern of Fig. 11f. The curve represents the second load step (σ = 25,400 psi = 175 MPa), prior to any evidence of yielding of the aluminum. The transverse displacements are very small. In this case, the initial pattern (the fringe pattern for no load) showed a uniform fringe shift of ΔN_y = 0.34 fringes across the adhesive thickness. This means that the adhesive increased in thickness by 0.34/f, or 5.5 μin. (0.14 μm), between the

time of application of the specimen grating and the time of the test. Such expansion could result from a change in ambient temperature, a change in moisture content, or both. It was accounted for by the relationship shown in Fig. 15, specifically, by subtracting 5.5 μin. from the displacement increments determined from Fig. 11f.

The transverse displacement in the adhesive, ΔV, goes to zero at about 0.12 inches (3.0 mm) from A, or about 14 times the adhesive thickness. The peak tensile displacement across the adhesive thickness is more than an order of magnitude larger than the (absolute value of) the largest compressive displacement.

One is tempted again to use the small strain relationship of Eq. 5, $\varepsilon_y = \Delta V/\Delta y$, for calculating average ε_y across AA', even though rotation of AA' is large. On the basis of Eq. 5, the average transverse strain on AA' is 0.021 m/m, or 2.1% strain. This might be compared with the averge gradient $\Delta U/\Delta y$ at AA', which is 5 times larger. A rigorous determination of ε_y at A requires the large strain relationship, Eq. 4b. It is suggested that the investigation should be conducted using specimens with much larger adhesive thickness to determine local effects near point A.

Figure 16 shows longitudinal strains ε_x along the boundary lines DAB and A'B', which include the adhesive/adherend interfaces. These are small strains, controlled largely by the aluminum adherends. Along DAB, ε_x exhibits a peak at point A for modest levels of average tensile stress. Curve I shows the peak displaced to the left of point A, and this is presumably caused by plastic deformation in the aluminum. While the onset of plastic deformation would be expected to occur at the same point as peak elastic strains, the evidence of Figs. 11d and e suggests that yielding is a heterogeneous

phenomenon and the material exhibits heterogeneous yielding properties. As such, yielding would not follow in exact harmony with elastic deformation.

The longitudinal strains on A'B' gradually increase to the level of those on DAB. For larger values of x than shown here, it is expected that the strain curves for the two interfaces would merge and then continue along a common curve.

Perfect representation of the displacements of the specimen surface would require a specimen grating of zero thickness. Otherwise, shear lag through the thickness of the grating material distorts the fringes in the immediate vicinity of abrupt changes of displacement gradients. Here, the fringes show slight rounding as they pass across the adhesive/adherend interface, while a more abrupt transition would be expected. The effect appears to extend about one grating thickness from the interface. In the present work this was 0.002 in. (0.05 mm). The excess fringe curvature in this zone was disregarded and fringes in the adherend were extrapolated across this zone to the interface. This compensated for the effect of shear lag in the grating. For future work, it would be attractive to develop techniques for applying thinner specimen gratings.

CONCLUSIONS

Two adhesive joint specimens were analyzed by experimental measurements. The longitudinal displacement across the adhesive thickness was nearly constant along the entire length of the joint. At the center of the lap joint, displacement ΔU and also shear strain γ_{xy} were nonlinear and time dependent functions of average shear stress in the adhesive. Transverse displacements across the adhesive thickness at the center of the lap was nonlinear, but exceedingly small. Longitudinal displacements and

strains ε_x along the adhesive/adherend boundary lines were very small compared to the shear displacements ΔU and shear strains γ_{xy} in the adhesive. Quantitative results are presented for all these effects.

The cracked lap shear specimen was stressed in 5 steps such that plastic deformation of the aluminum adherend began at the third step. The specimen exhibited much less creep and relaxation. Longitudinal displacements ΔU across the adhesive thickness decreased gradually to about 10% of its peak value at a distance of 0.5 in. (13 mm) from the joint discontinuity. Longitudinal displacements ΔU across the adhesive thickness was a nonlinear function of average tensile stress, but its time dependence was small. Transverse displacements across the adhesive thickness were small, but peaked at the joint discontinuity; here, the gradients $\Delta V/\Delta y$ and $\Delta U/\Delta y$ (averaged across the adhesive thickness) were in the ratio 1:5. Longitudinal strains ε_x along the adhesive/adherend boundary lines peaked near the joint discontinuity, where first evidence of plastic deformation in the aluminum was observed. Quantitative results are presented.

Strain concentrations near the joint discontinuities, for both normal and shear strains, are either very small or very highly localized. Future work on their detailed analysis is suggested. Enlarged models of the joints should be used for those investigations.

Moire interferometry is an excellent technique to measure in-plane displacements of adhesive joints. Its subwavelength sensitivity and very high spatial resolution allow unprecedented opportunities for whole-field analyses of joints.

ACKNOWLEDGEMENTS

The authors appreciate very helpful discussions with Professor H. L. Brinson of VPI&SU and Dr. W. S. Johnson of NASA Langley Research Center.

REFERENCE

1. Post, D., "Moire Interferometry at VPI & SU", Experimental Mechanics, 23(2), 203-211 (June 1983).

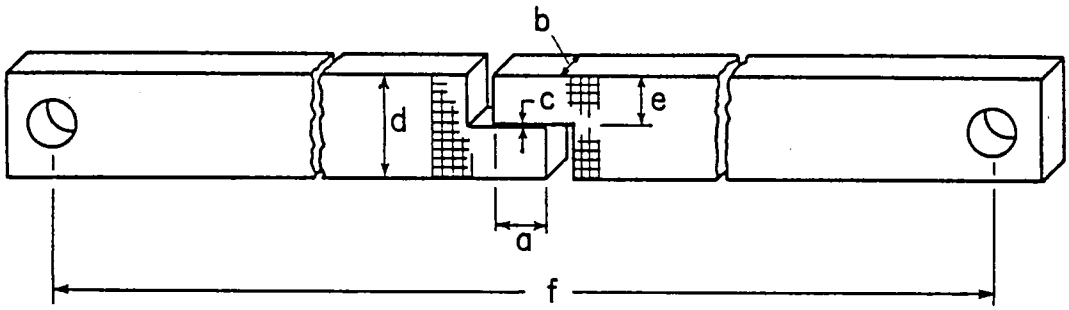

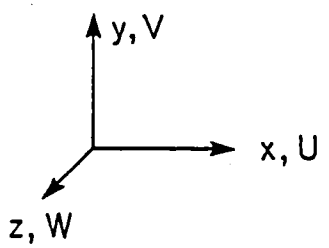

THICK ADHEREND LAP JOINT SPECIMEN

	in.	mm
a	0.344	8.75
b	0.261	6.63
c	0.0087	0.22
d	0.744	18.90
e	0.368	9.34
f	8.0	200.

Materials, both specimens
Adherend: Aluminum 2024-T3
Adhesive: Rubber modified epoxy FM-73M, Cured at 250°F.

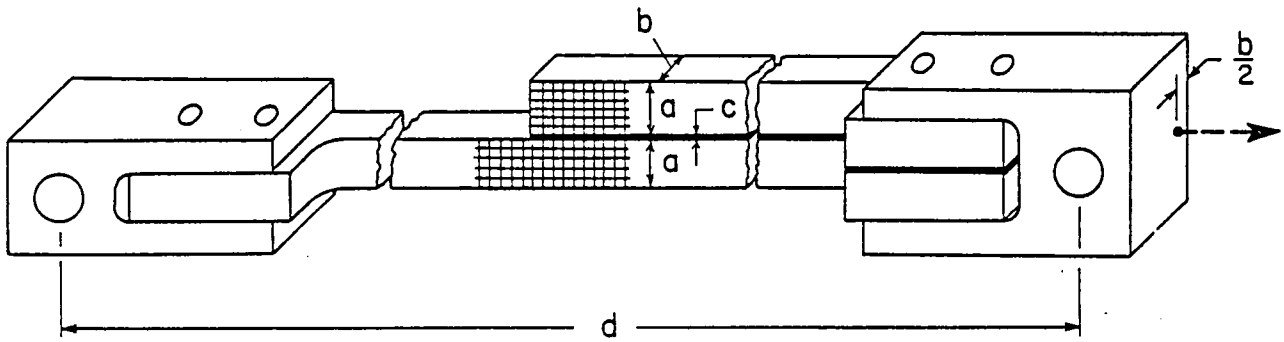

CRACKED LAP SHEAR SPECIMEN

	in.	mm
a	0.197	5.00
b	0.149	3.78
c	0.0083	0.21
d	10.0	250.

Fig. 1 Specimen dimensions and materials. Grid represents the crossed-line specimen grating employed for displacement measurements.

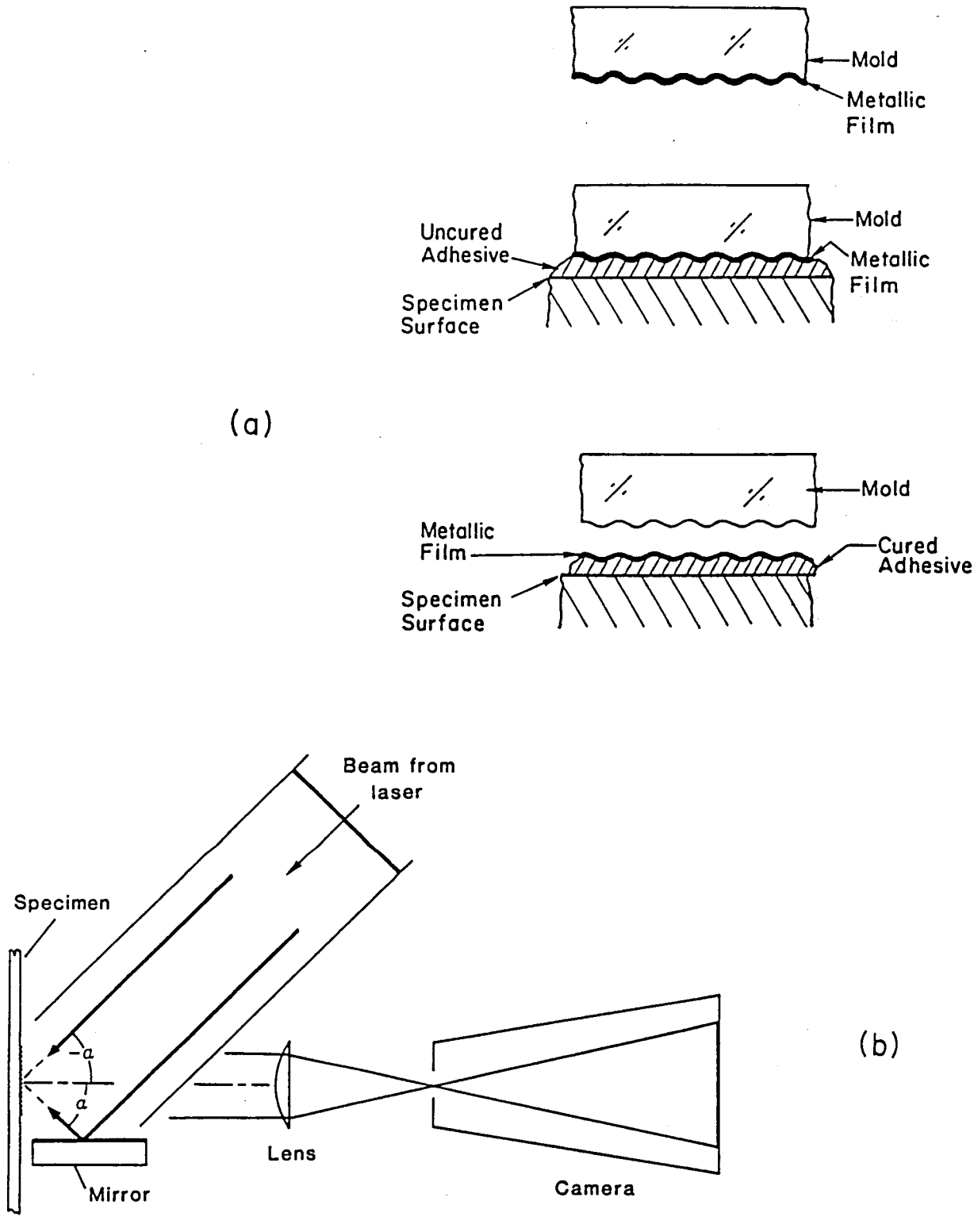

Fig. 2 (a) Replication technique to form a high-frequency, high reflectance grating on the specimen.
(b) Optical arrangement for moire interferometry.

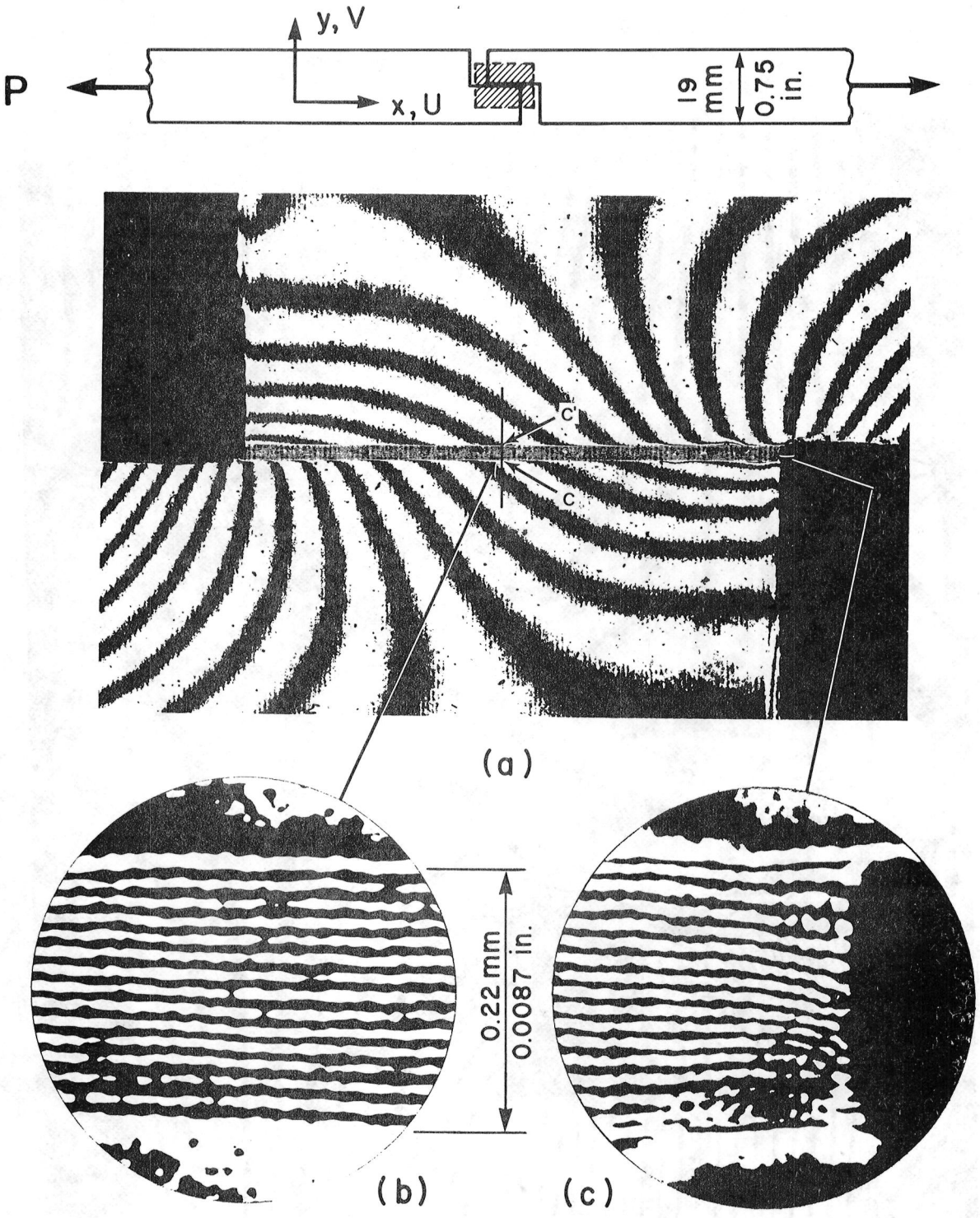

Fig. 3 (a) U displacement field from preliminary test.
(b) Enlarged view at center of lap.
(c) Enlarged view at end of lap.
Average shear stress in lap = τ = P/lap area = 2080 psi.
Pattern taken 1 minute after load application.

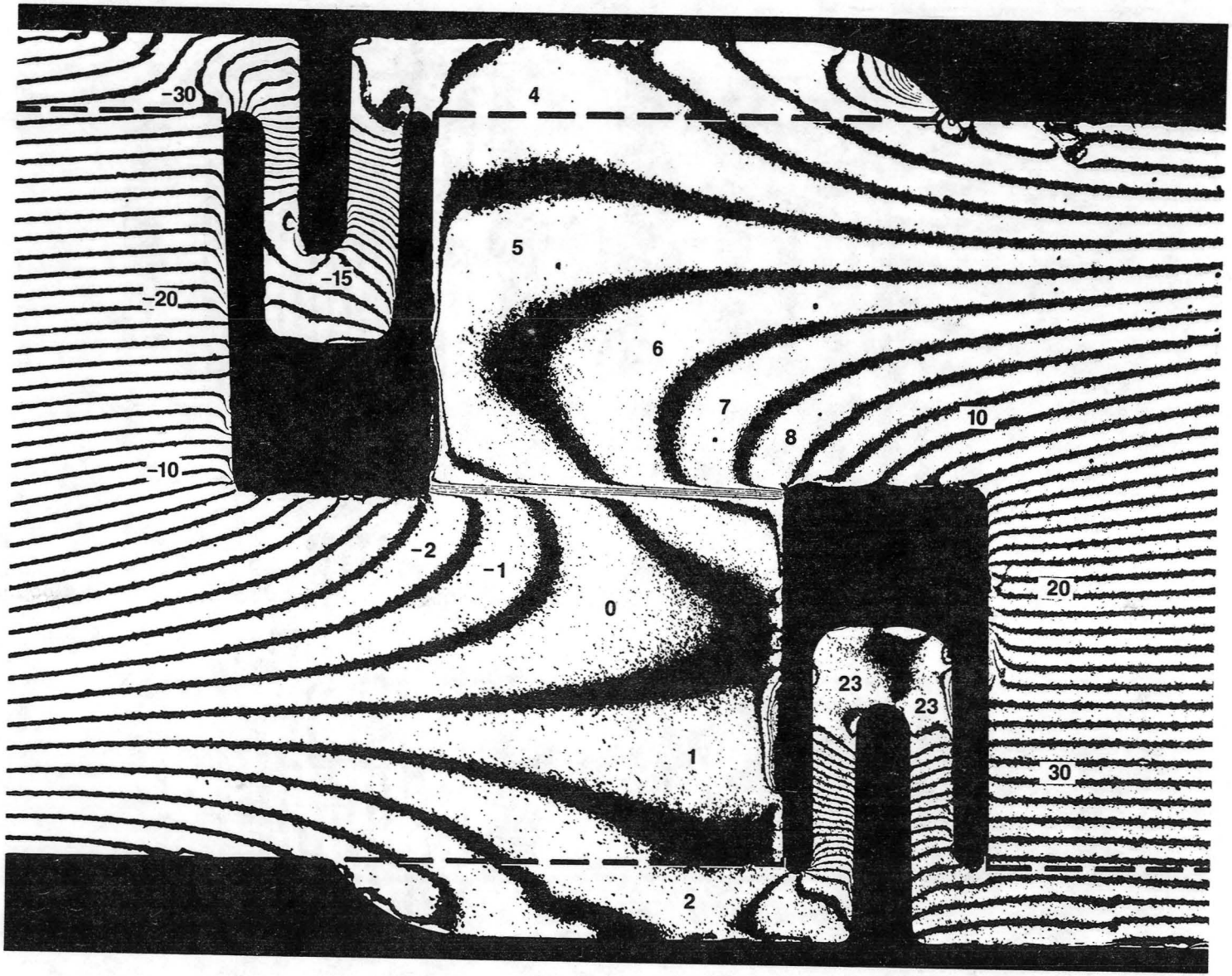

Fig. 4a U displacement field for the thick adherend lap joint specimen. Omega-shaped bridges span the gap between adherends. Numbers signify fringe orders N_x. τ = 995 psi; 17 minutes after load application.

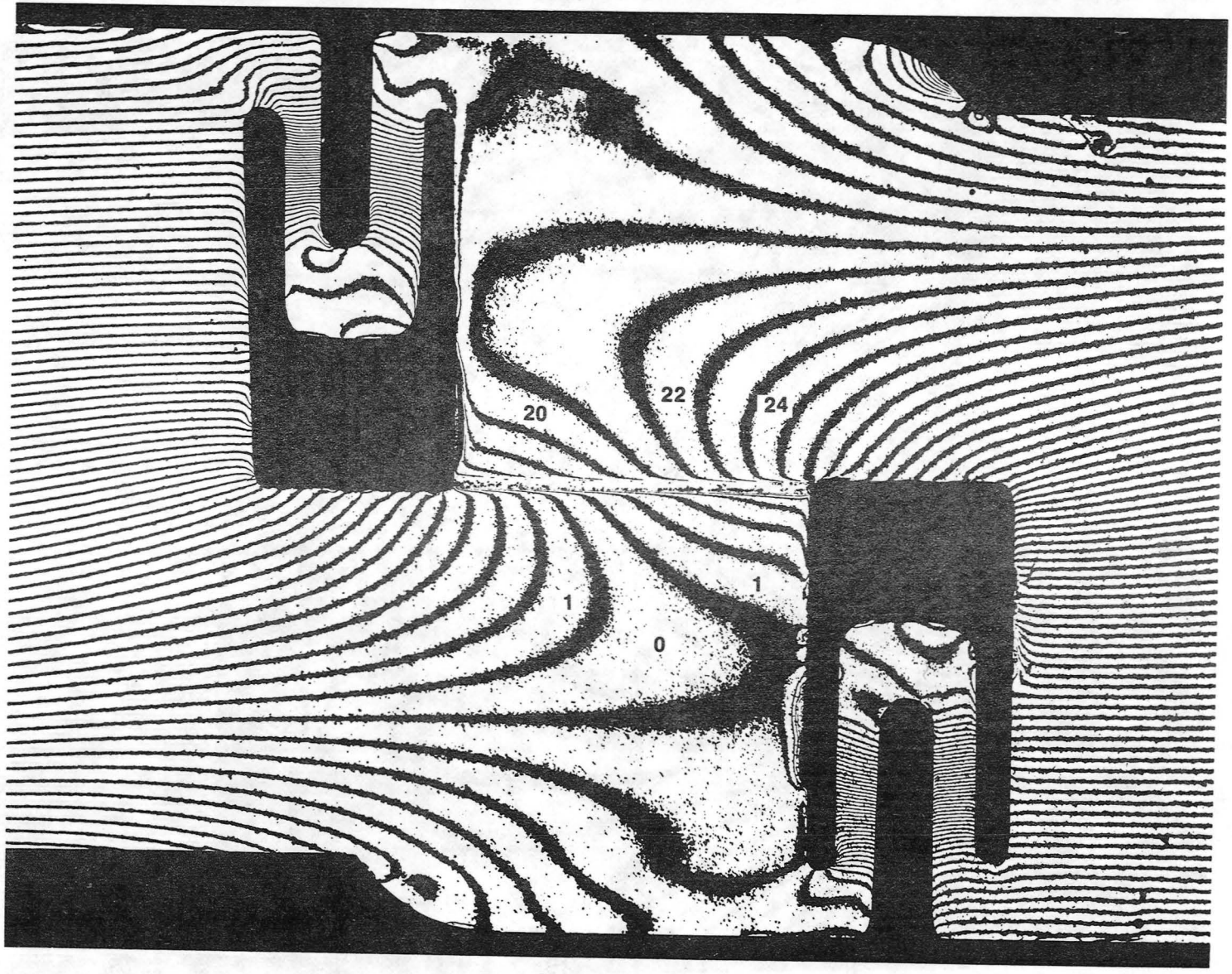

Fig. 4b U displacement field. τ = 1990 psi; 16 minutes after load.

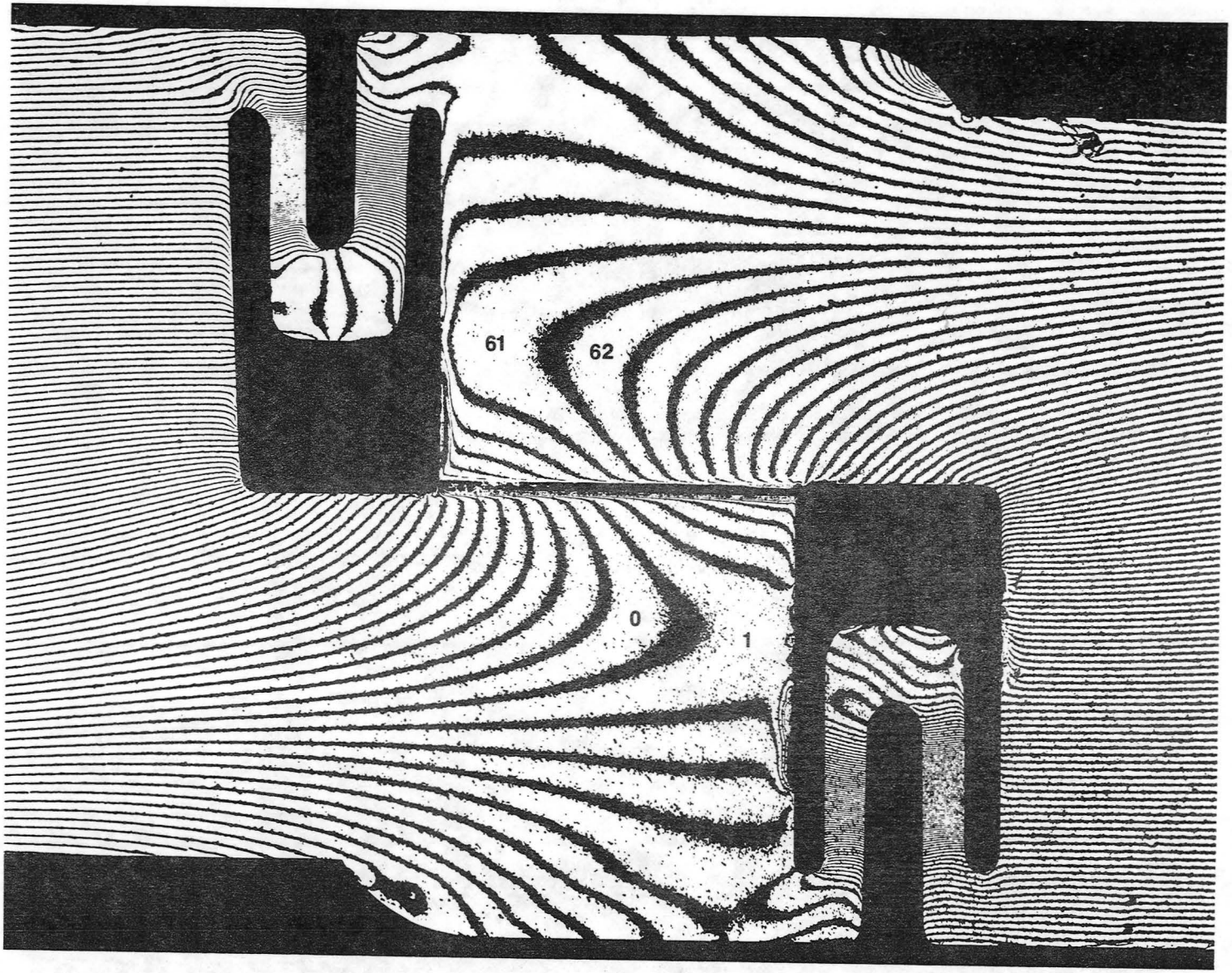

Fig. 4c U displacement field. τ = 2770 psi; 16 minutes after load.

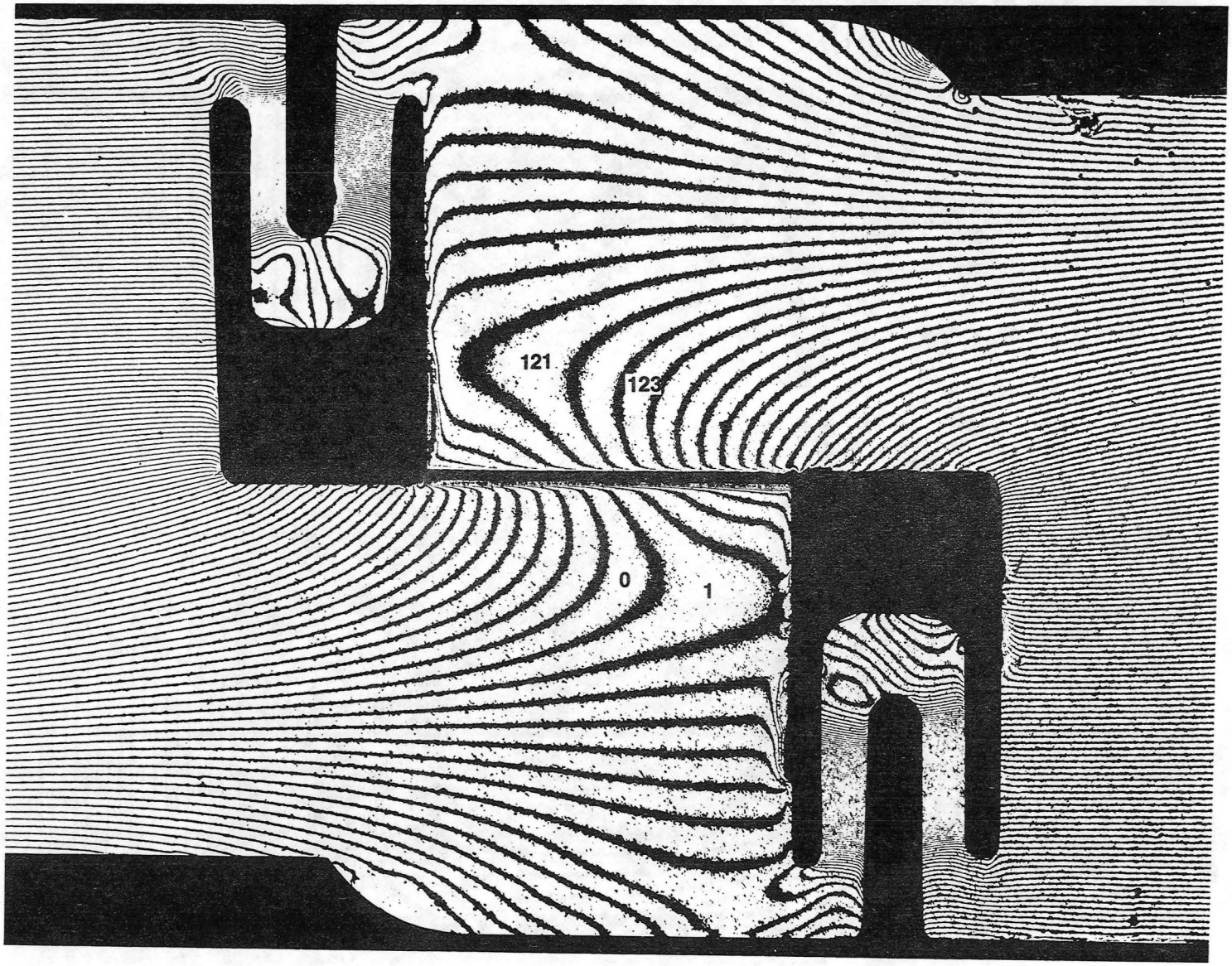

Fig. 4d U displacement field. τ = 3190 psi; 16 minutes after load.

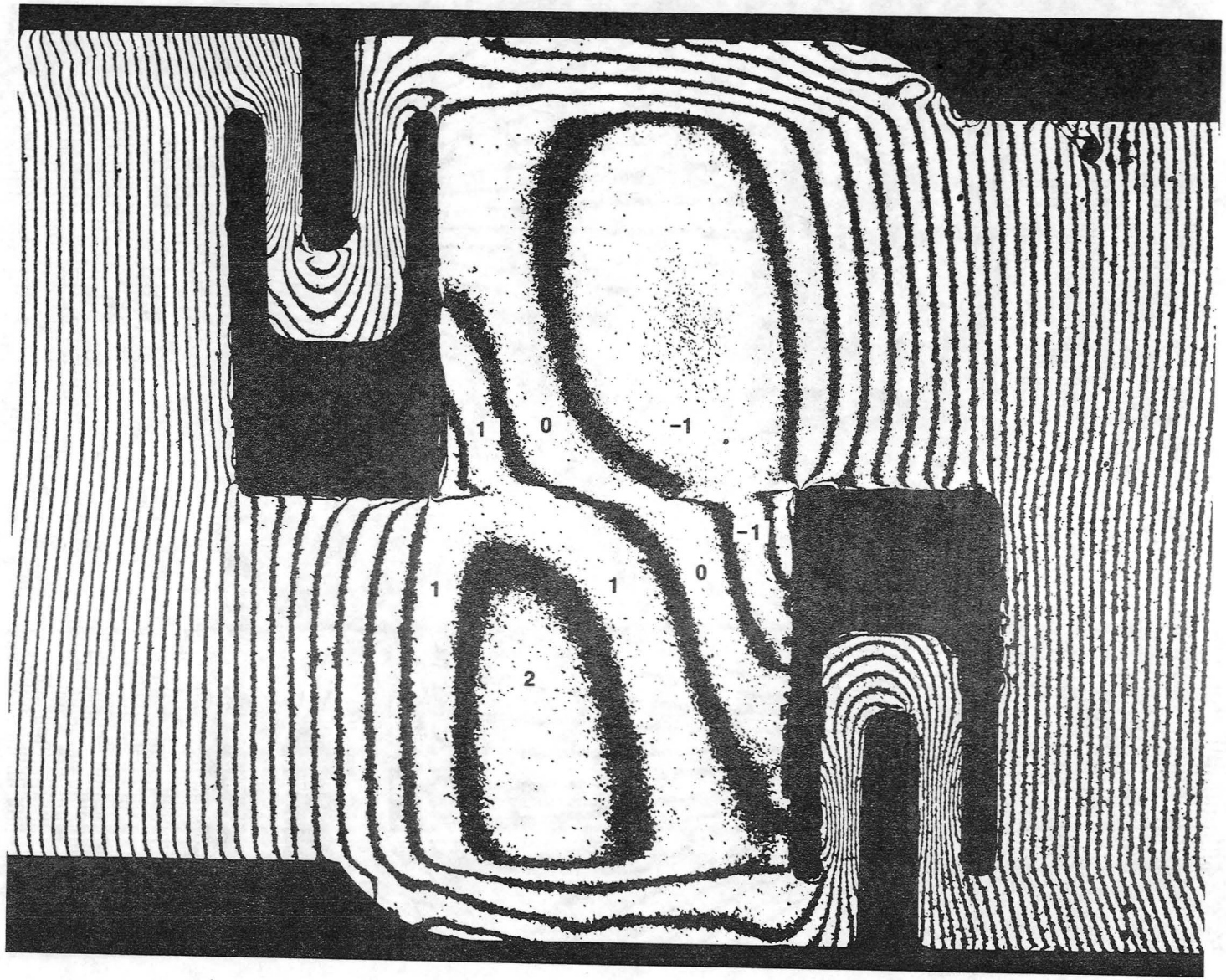

Fig. 4e V displacement field. Numbers signify N_y. τ = 1990 psi; 17 minutes after load.

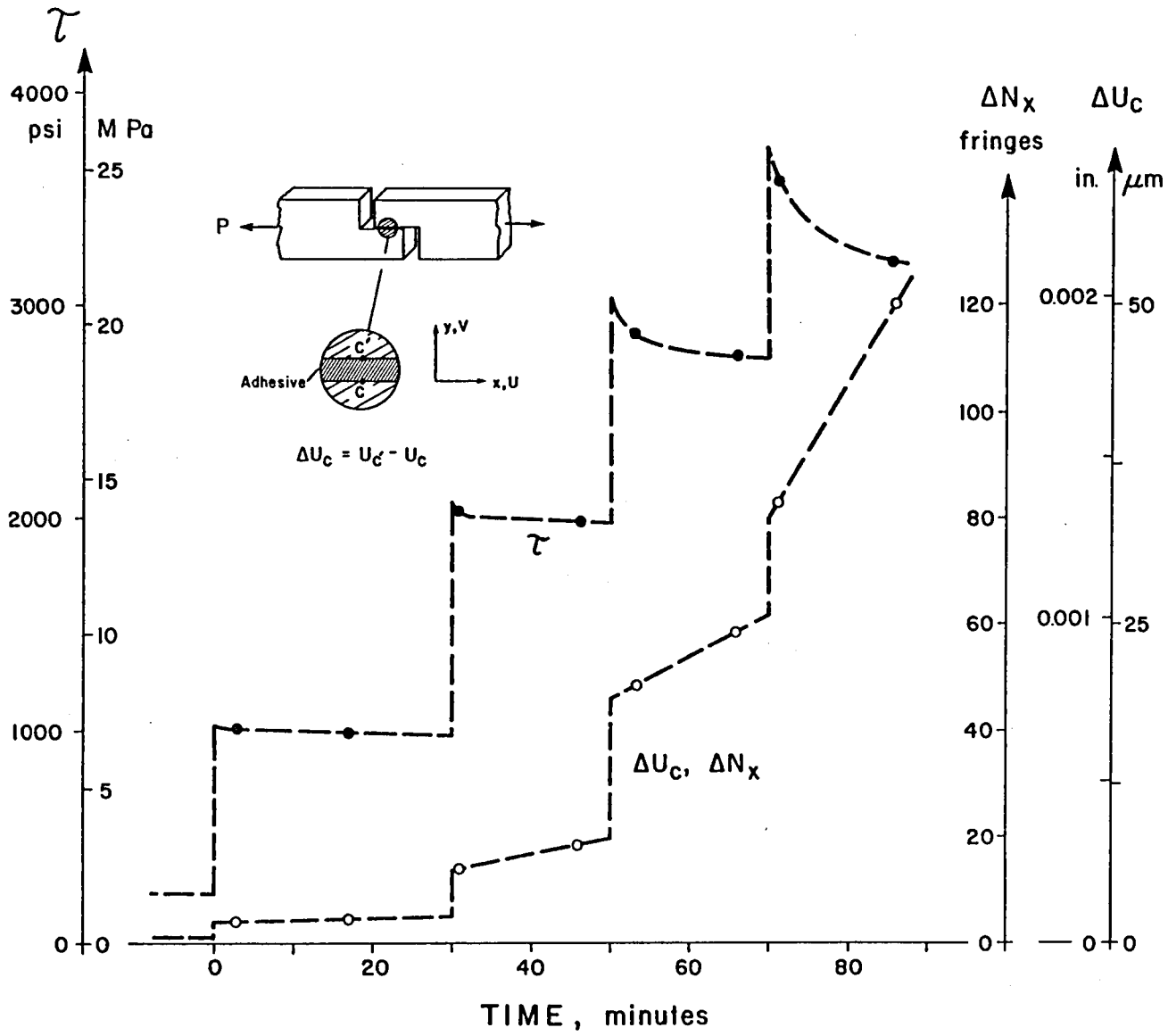

Fig. 5 Shear stress and displacement history for the thick adherend lap joint specimen.

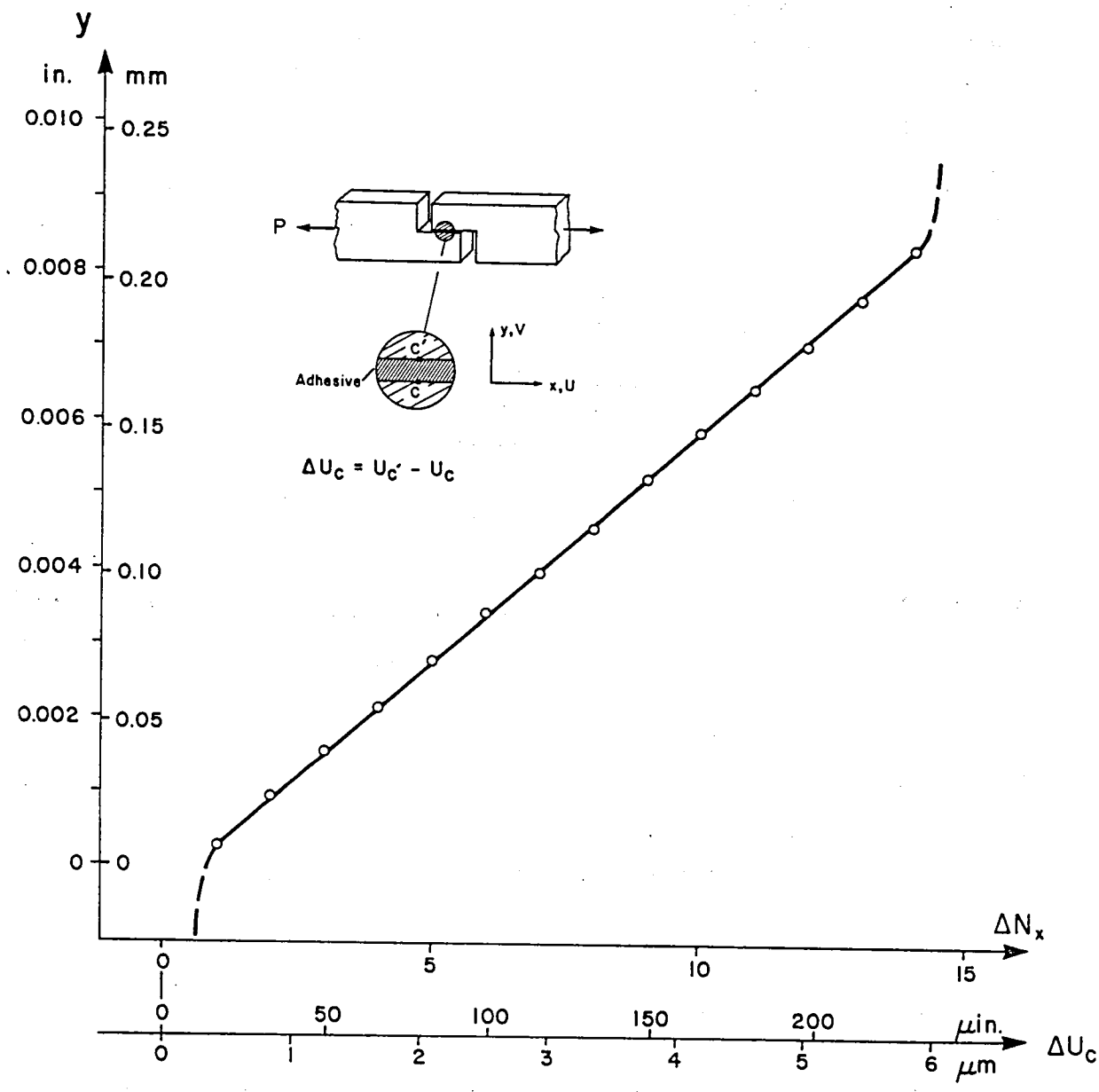

Fig. 6 ΔU vs. y in adhesive along line CC'. Data was taken from Fig. 3b (preliminary test). τ = 2080 psi; 1 minute after load application.

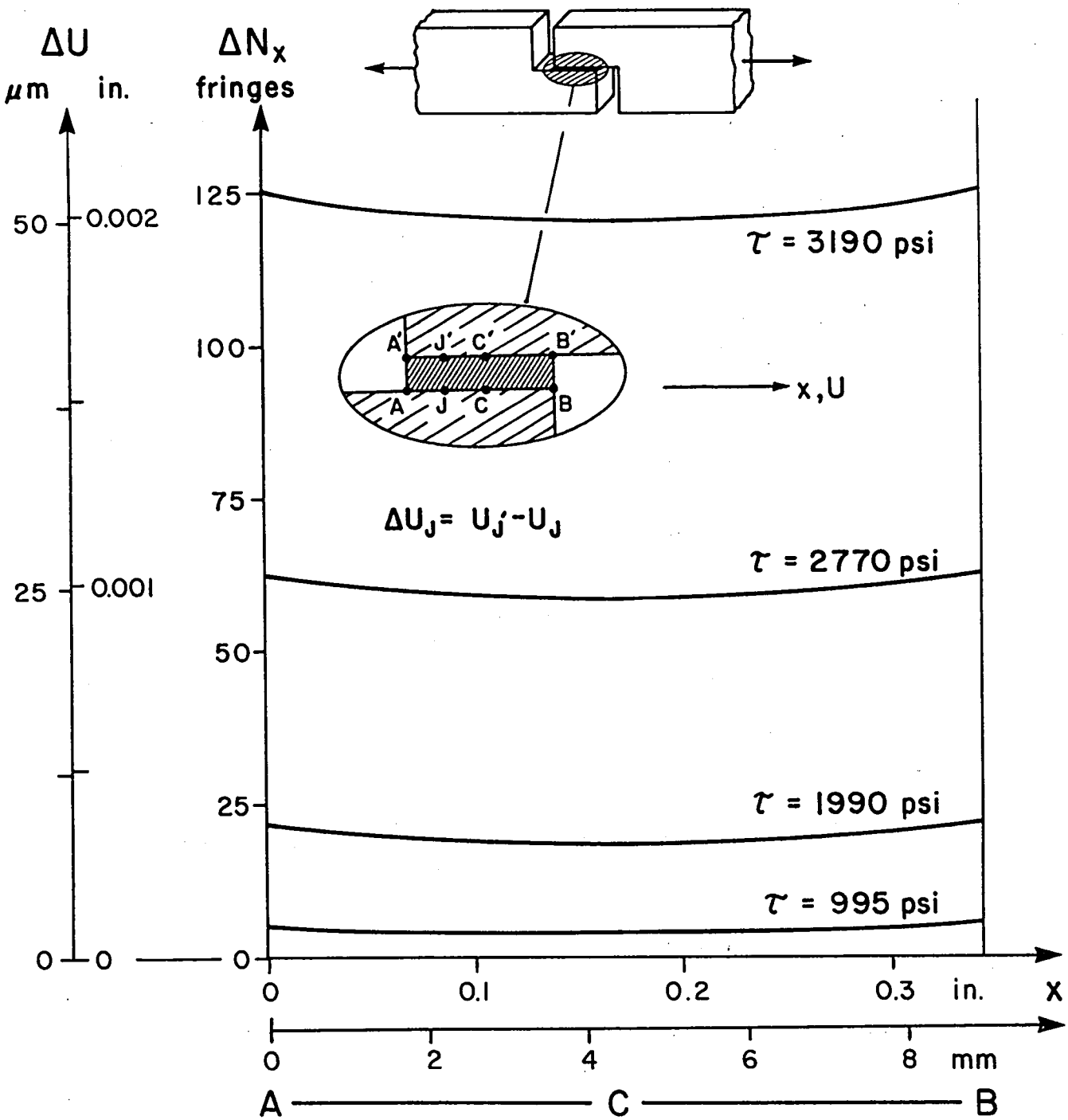

Fig. 7 ΔU across adhesive thickness vs. x; 16 minutes (approximately) after each load application.

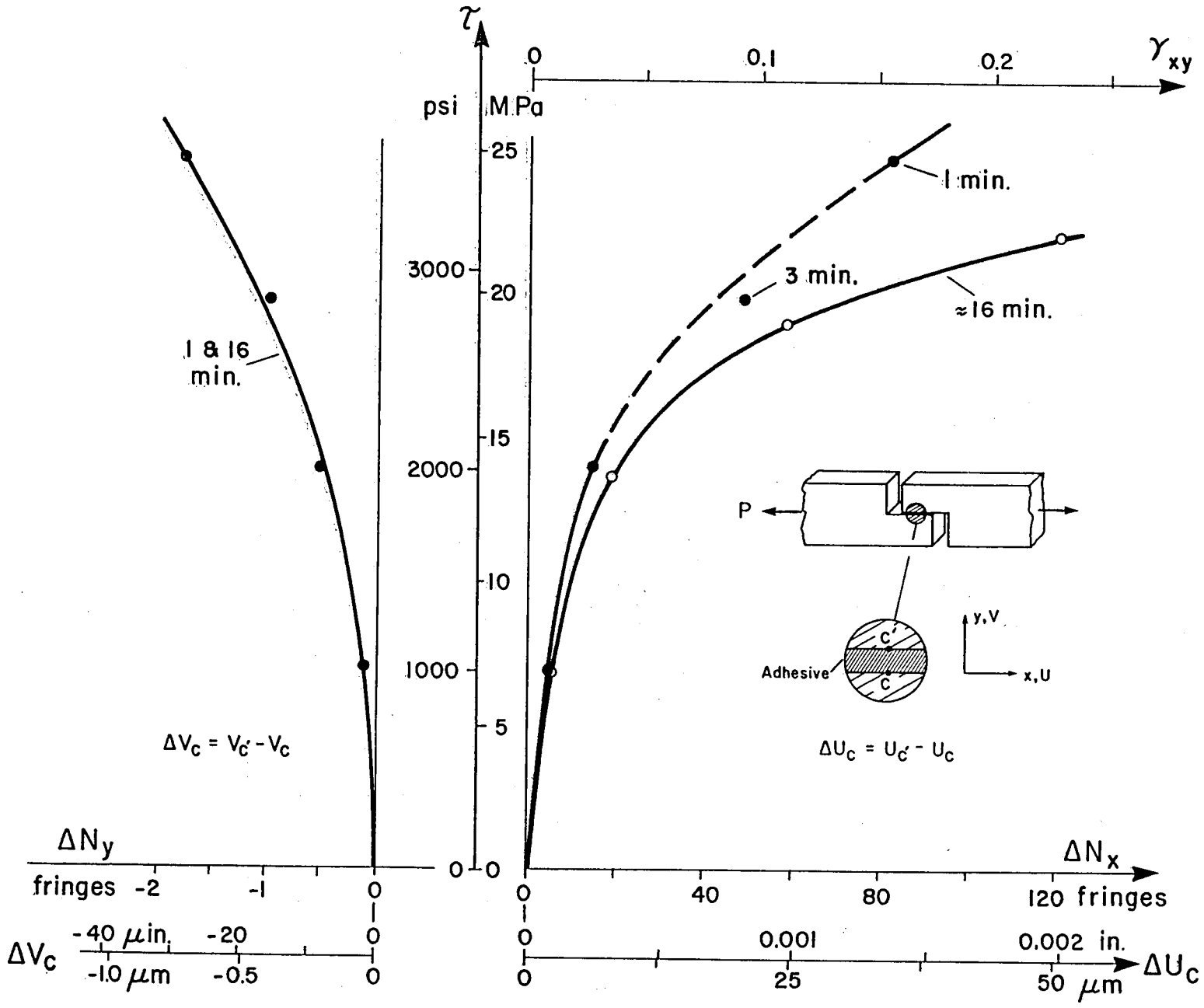

Fig. 8 ΔU, ΔV and γ_{xy} across adhesive thickness at center of lap vs. average shear stress, τ; 1 and 16 minutes (approximately) after each load application.

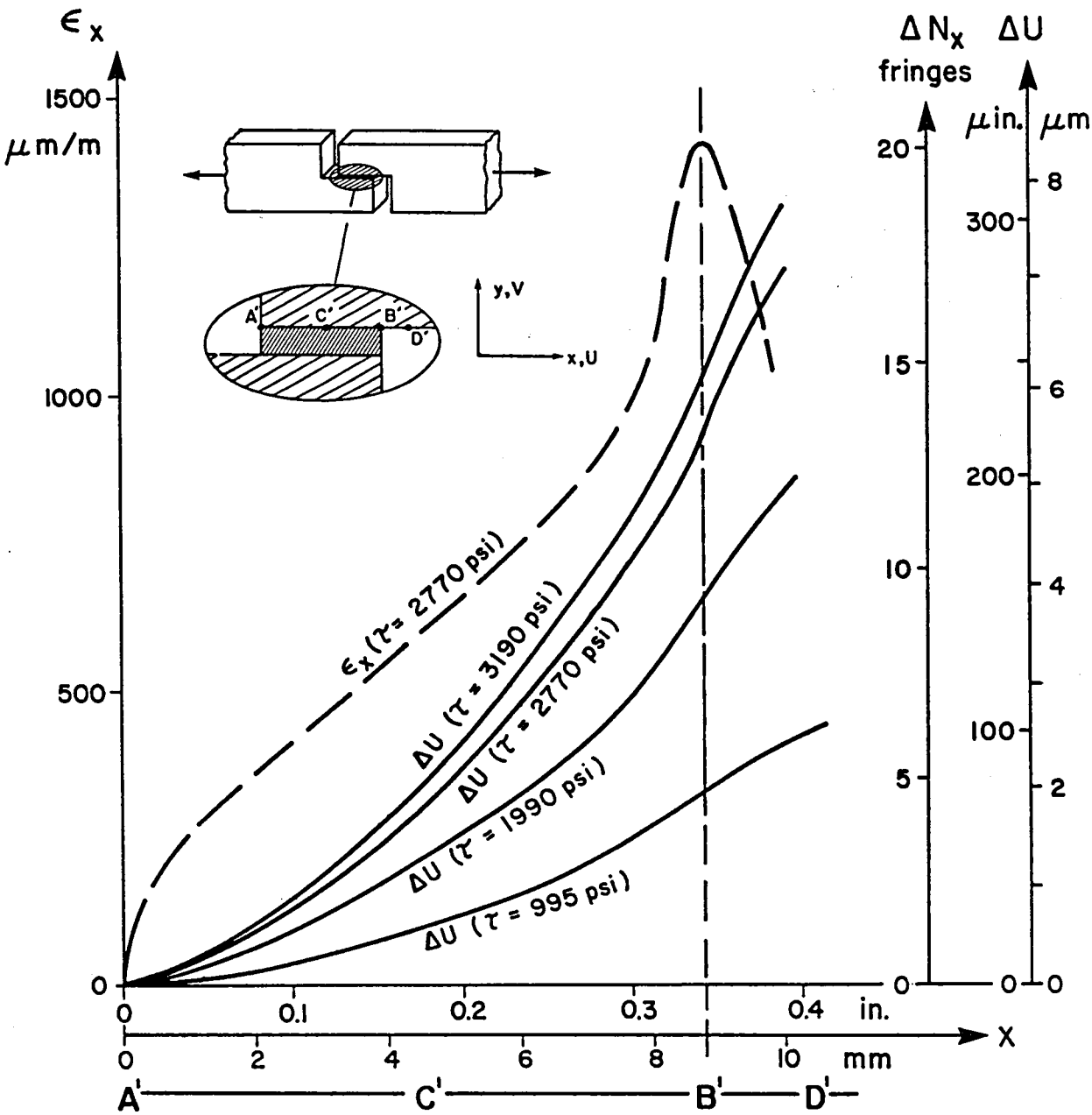

Fig. 9 ΔU and ϵ_x vs. x along adhesive/adherend interface A'C'B', and along B'D'; 16 minutes (approximately) after each load application.

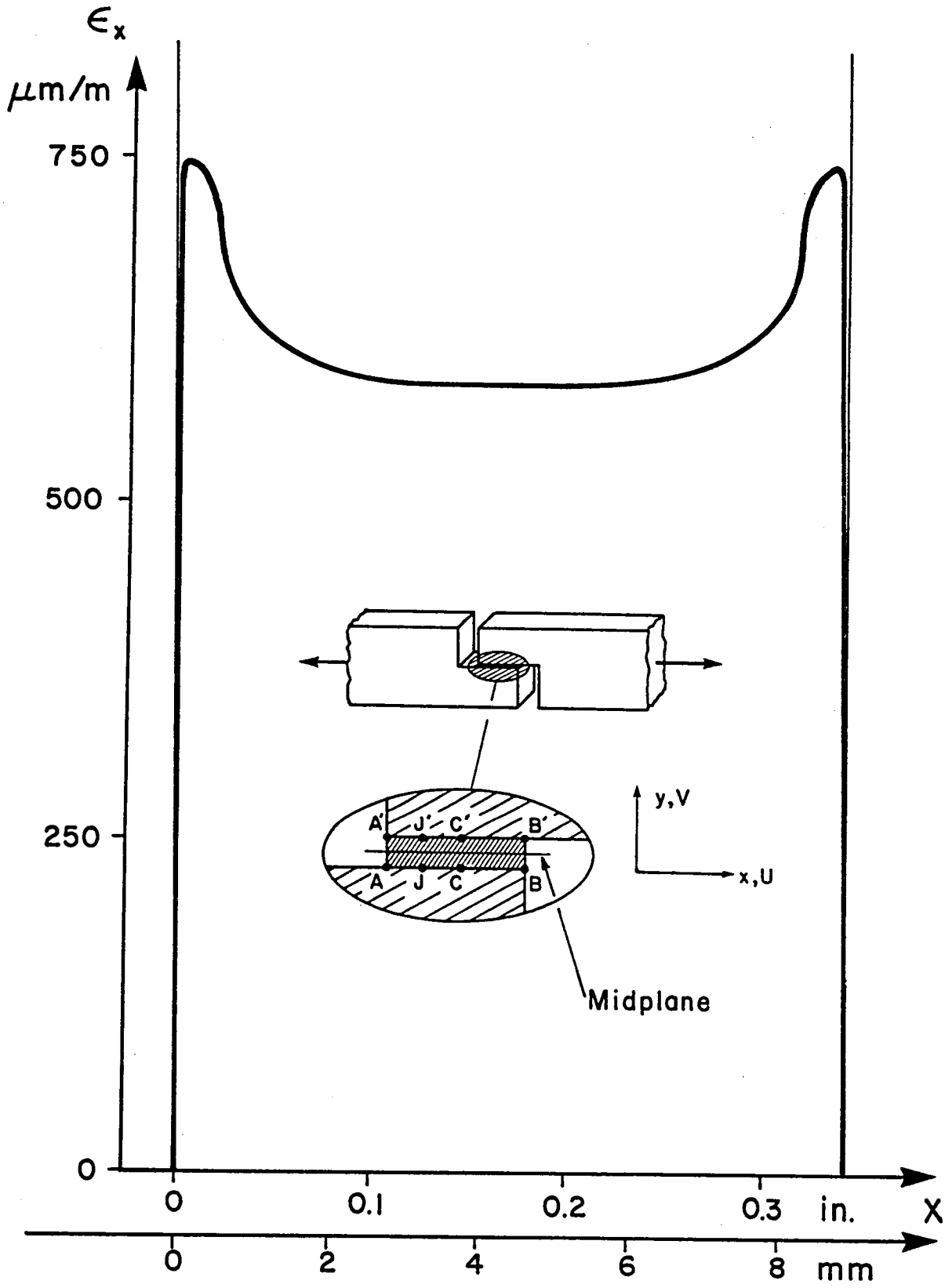

Fig. 10 ϵ_x vs. x at the midplane of the adhesive, assuming a linear variation of ϵ_x from any generic point J to J'.

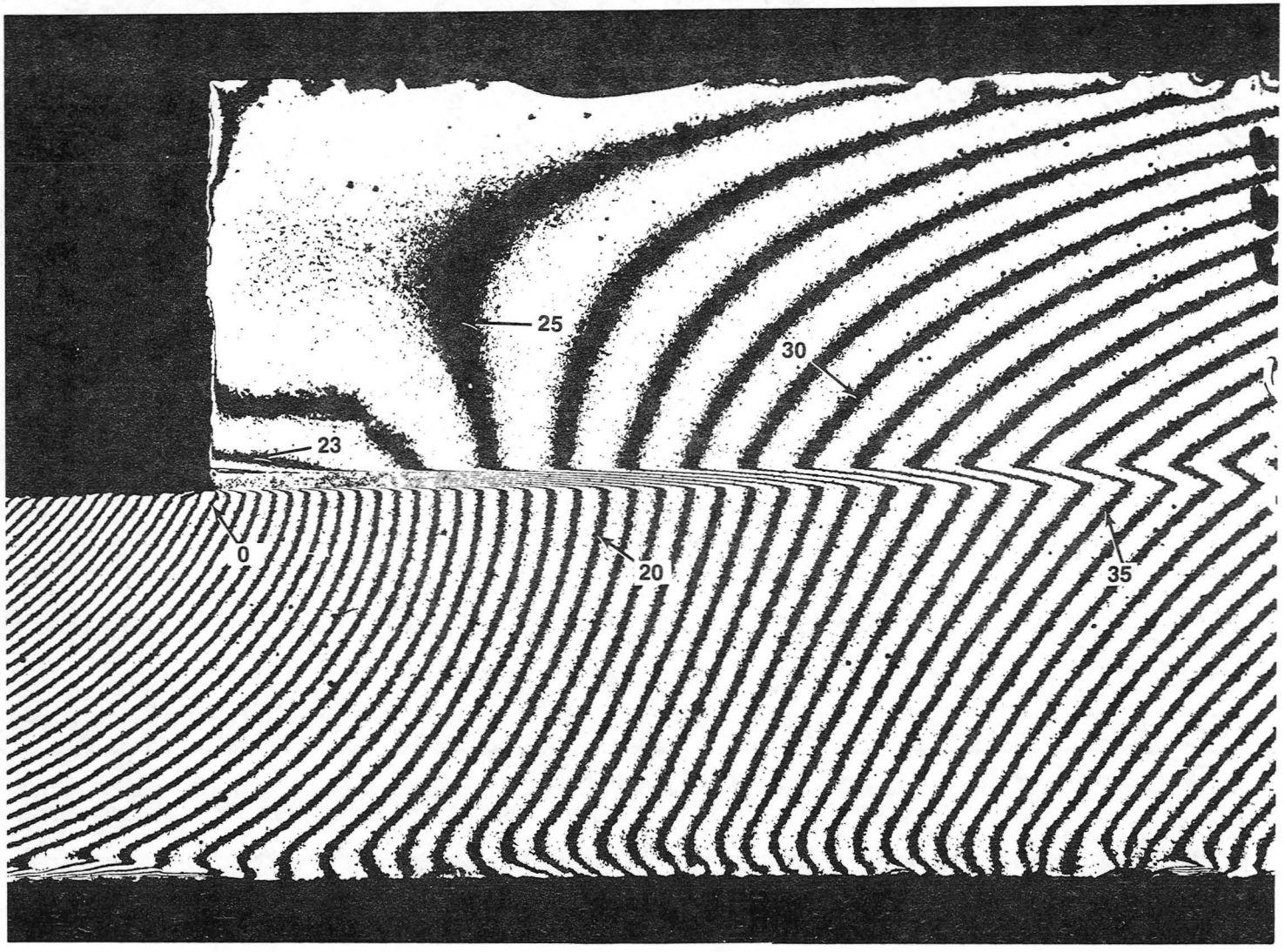

Fig. 11a U displacement field for the cracked lap shear specimen. Numbers signify fringe orders, N_x. Average tensile stress on longer adherend = σ = 12,900 psi. Pattern taken 7 minutes after load applicaton.

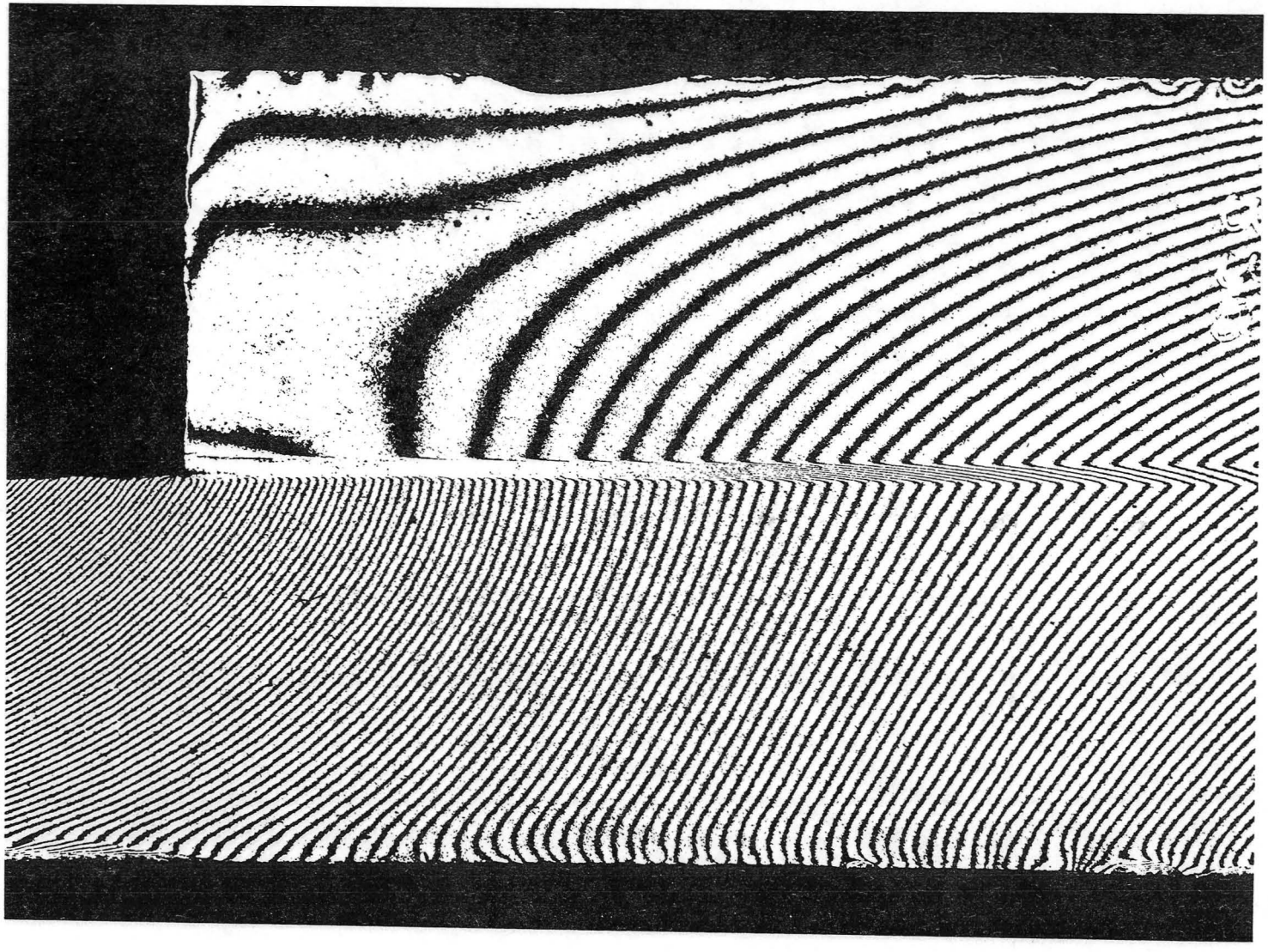

Fig. 11b U displacement field. σ = 25,400 psi; 10 minutes after load.

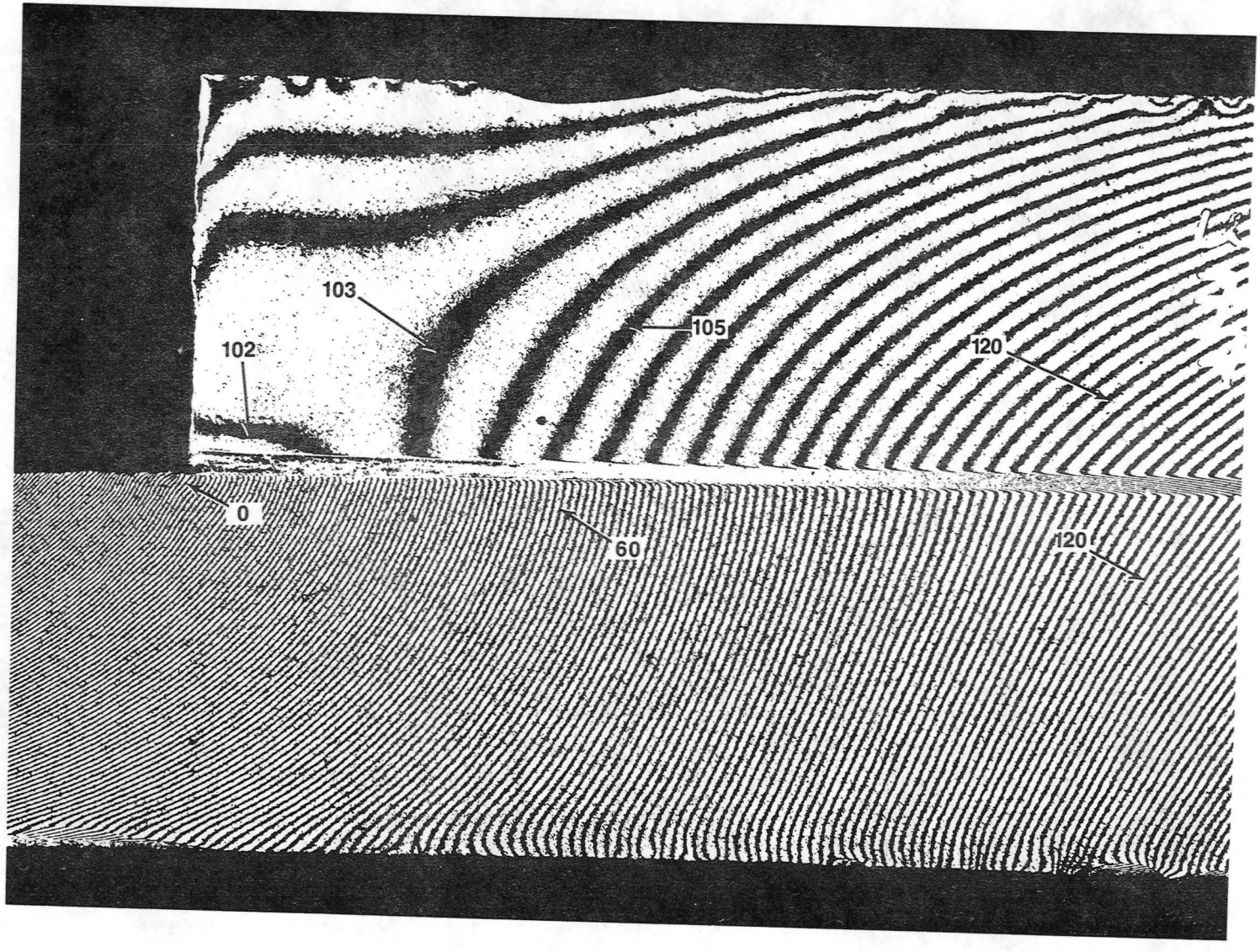

Fig. 11c U displacement field. σ = 38,300 psi; 7 minutes after load.

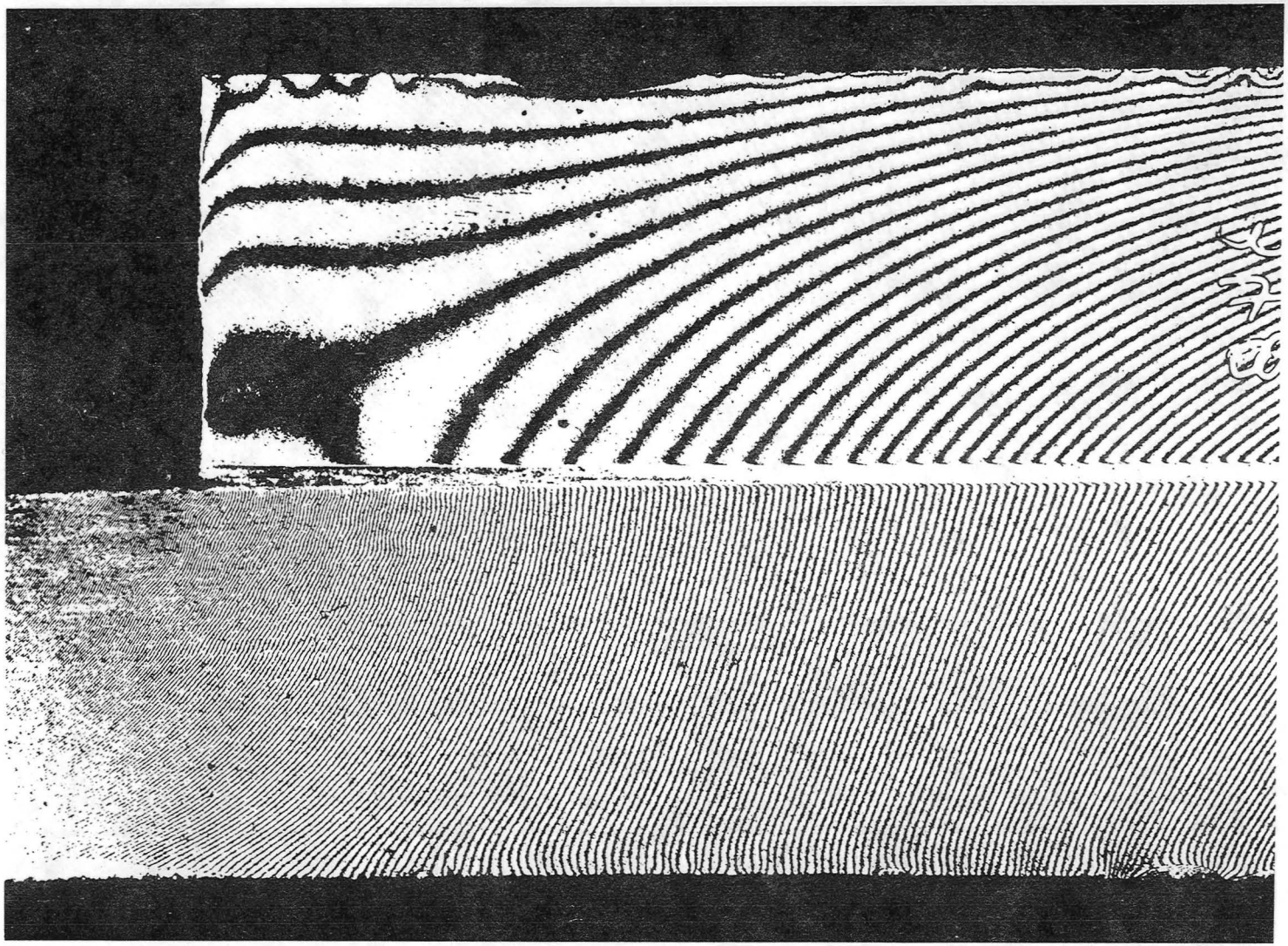

Fig. 11d U displacement field. σ = 51,800 psi; 7 minutes after load.

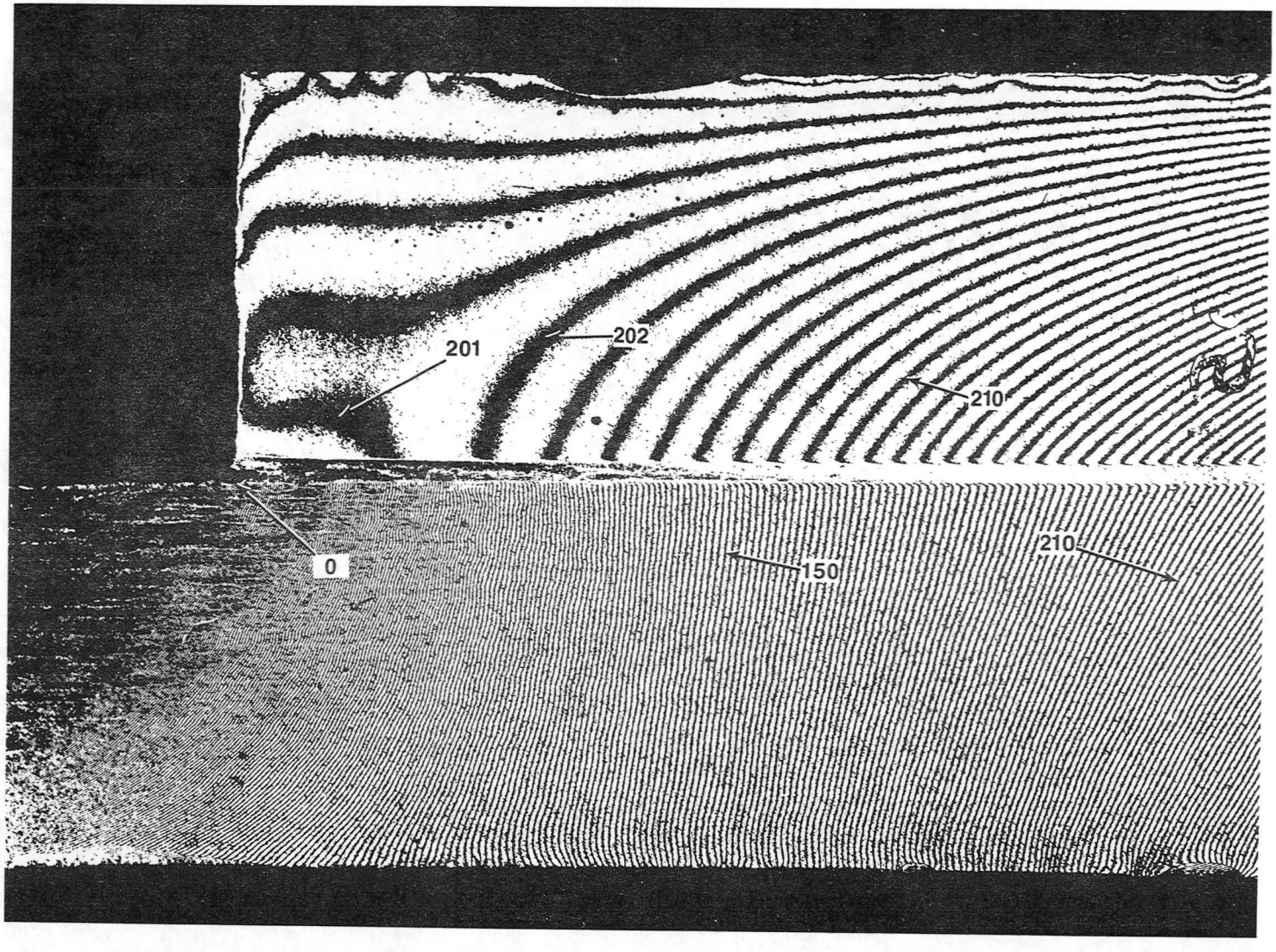

Fig. 11e U displacement field. σ = 57,200 psi; 7 minutes after load.

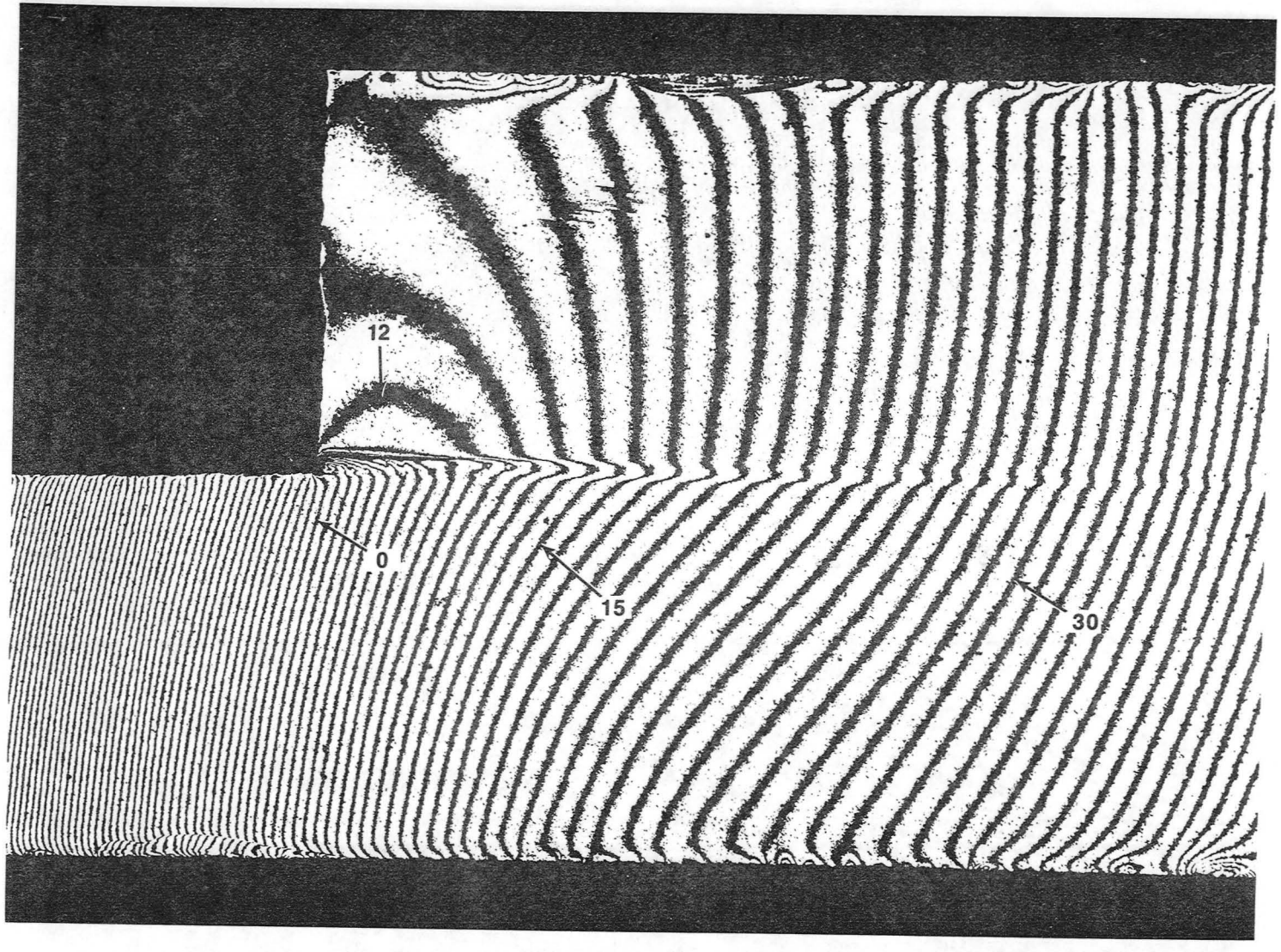

Fig. 11f V displacement field. Numbers signify N_y. σ = 25,400 psi; 1 minute after load.

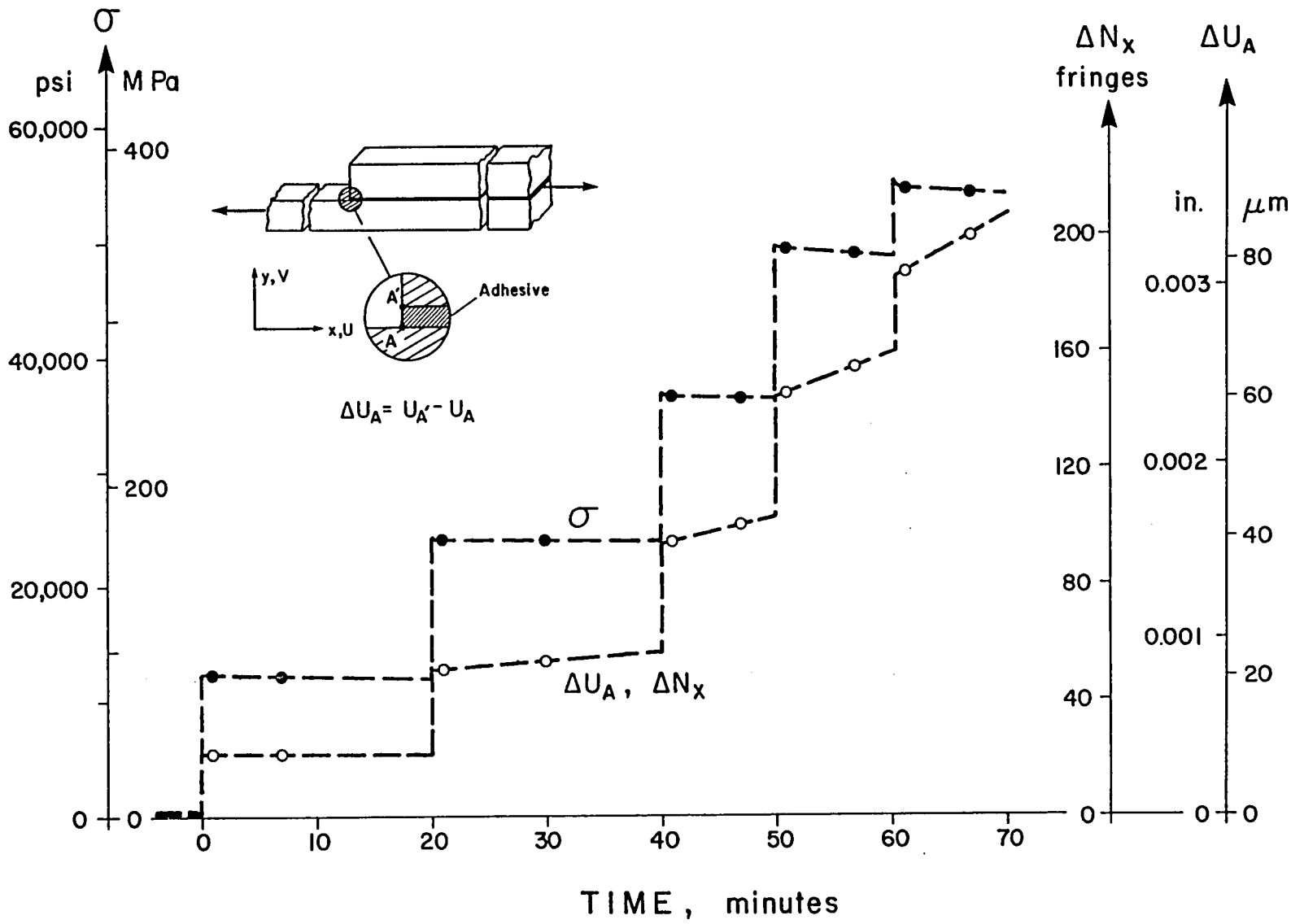

Fig. 12 Tensile stress and displacement history for the cracked lap shear specimen.

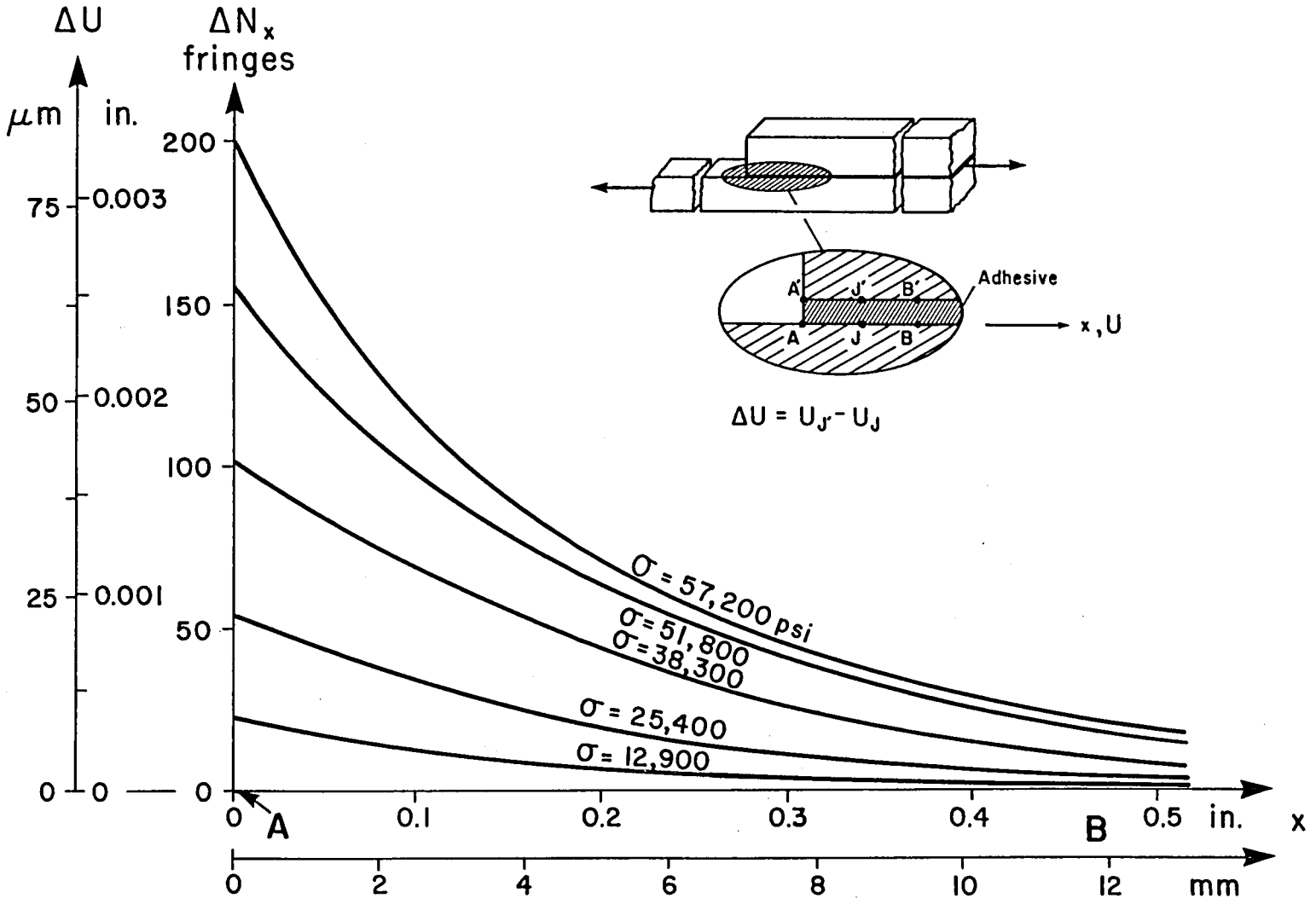

Fig. 13 ΔU across adhesive thickness vs. x; 7 minutes (approximately) after load application.

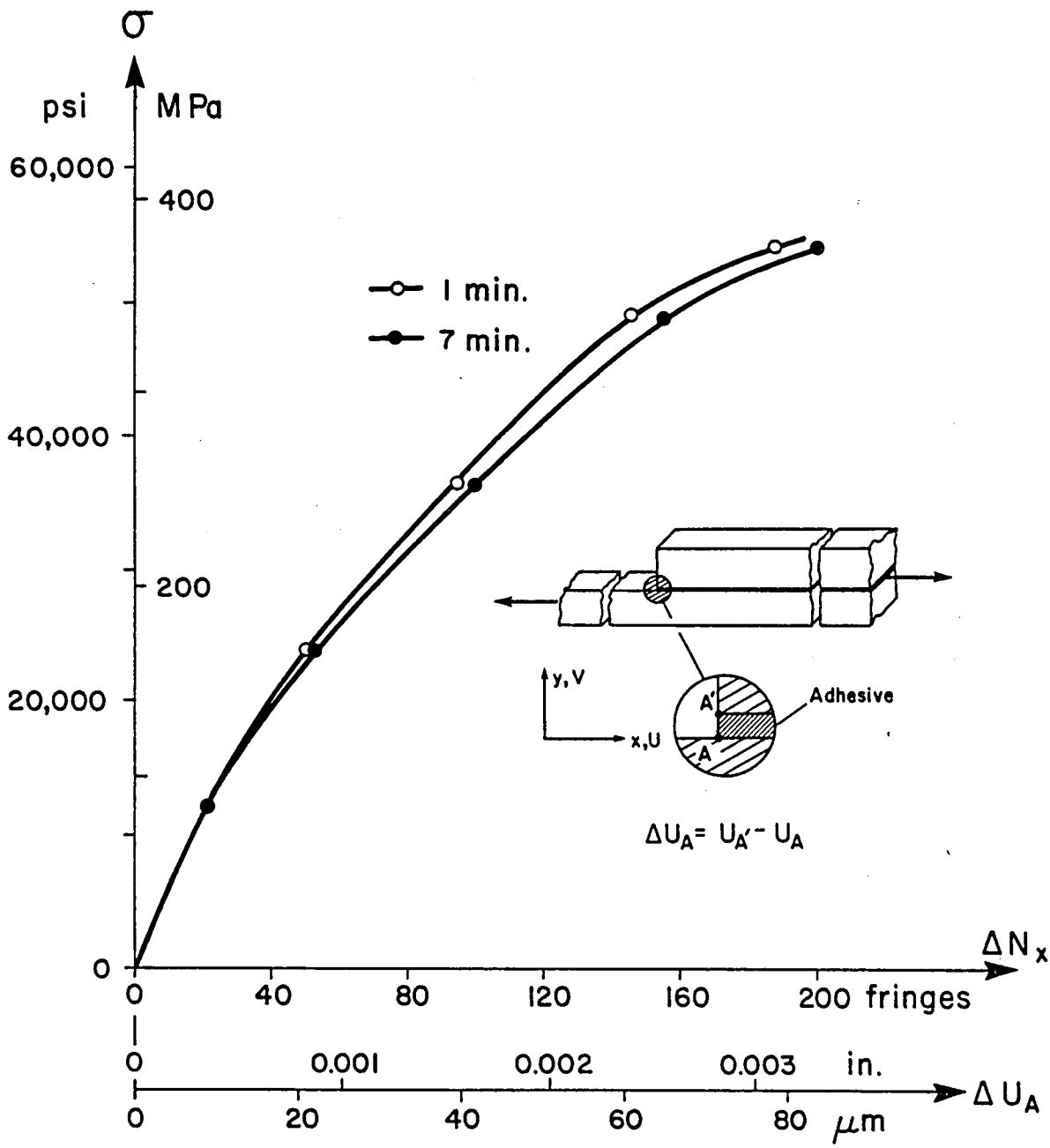

Fig. 14 ΔU across adhesive thickness at A vs. average tensile stress, σ; 1 and 7 minutes (approximately) after load application.

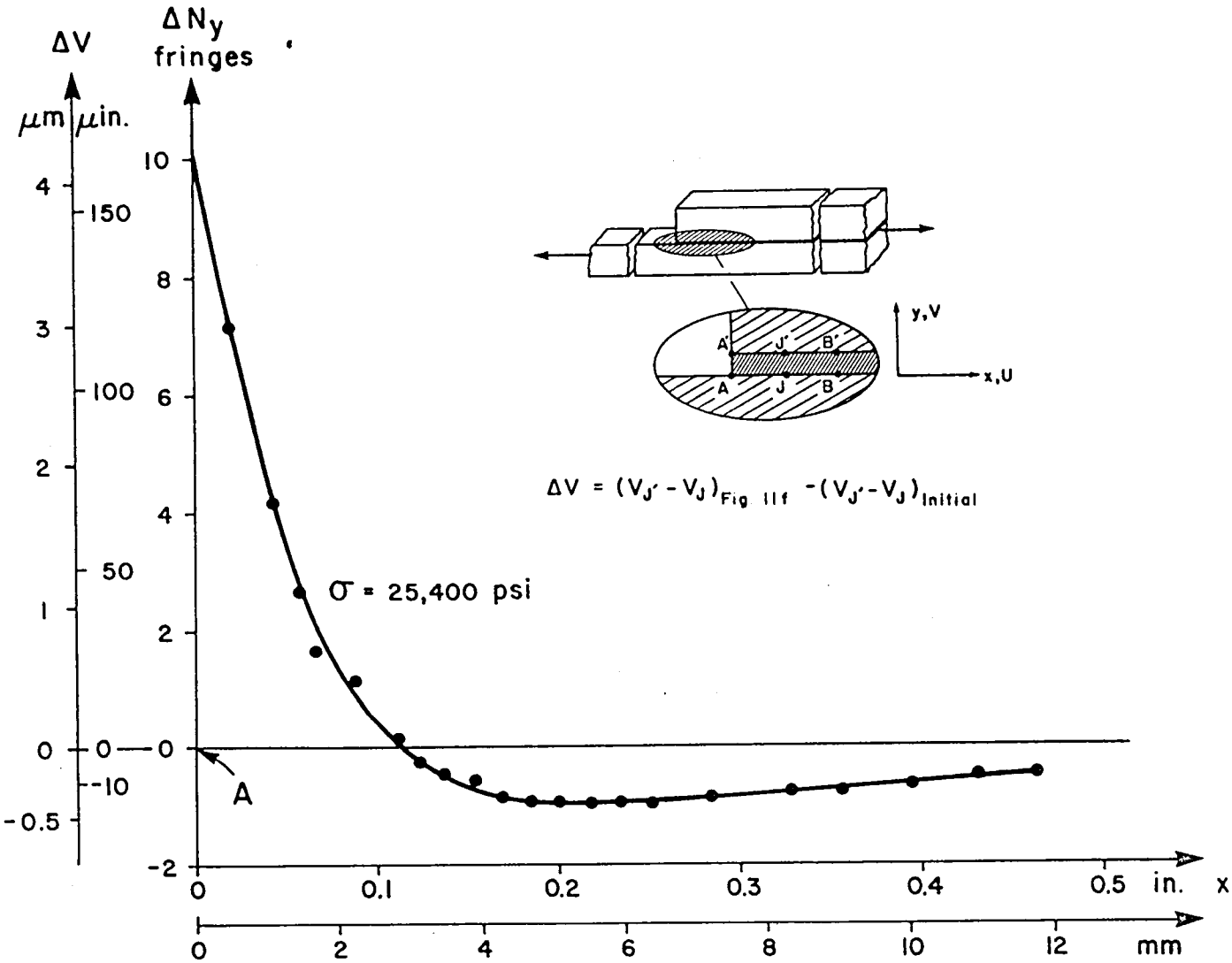

Fig. 15 ΔV across adhesive thickness vs. x; 1 minute after load application. Results for 7 minutes after load application are virtually identical to these.

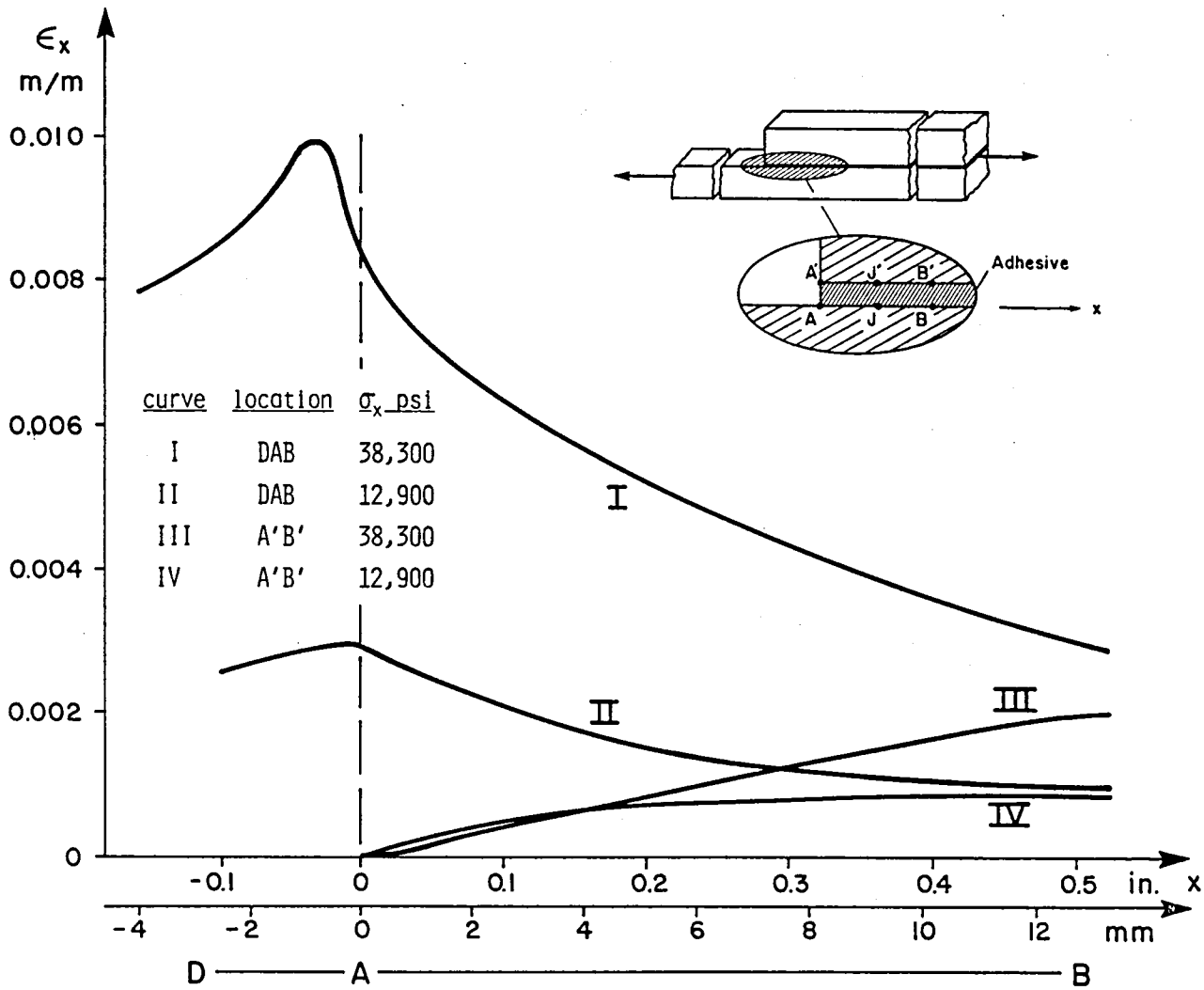

Fig. 16 ϵ_x vs. x along DA and along adhesive/adherend interfaces AB and A'B'; 7 minutes after load application.

1. Report No.	2. Government Accession No.	3. Recipient's Catalog No.
NASA CR-172474		

4. Title and Subtitle	5. Report Date
DEFORMATIONS AND STRAINS IN ADHESIVE JOINTS BY MOIRE INTERFEROMETRY	October 1984
	6. Performing Organization Code

7. Author(s)	8. Performing Organization Report No.
Daniel Post, Robert Czarnek, Judy Wood, Duksung Joh, and Steven Lubowinski	
	10. Work Unit No.

9. Performing Organization Name and Address	11. Contract or Grant No.
Virginia Polytechnic Institute and State University Engineering Science and Mechanics Department Blacksburg, VA 24061	NAG1-227
	13. Type of Report and Period Covered

12. Sponsoring Agency Name and Address	13. Type of Report and Period Covered
National Aeronautics and Space Administration Washington, DC 20546	Contractor Report
	14. Sponsoring Agency Code

15. Supplementary Notes

Langley technical monitor: Dr. W. Steven Johnson

16. Abstract

Displacement fields in a thick adherend lap joint and a cracked lap shear specimen were measured by high-sensitivity moire interferometry. Contour maps of in-plane U and V displacements were obtained across adhesive and adherend surfaces. Loading sequences ranged from modest loads to near-failure loads. Quantitative results are given for displacements and certain strains in the adhesive and along the adhesive/adherend boundary lines. The results show non-linear displacements and strains as a function of loads or stresses; and they show viscoelastic or time-dependent response.

Moire interferometry is an excellent method for experimental studies of adhesive joint performance. Subwavelength displacement resolution of a few micro-inches, and spatial resolution corresponding to 1600 fringes/inch (64 fringes/mm), were obtained in these studies. The whole-field contour maps offer insights not available from local measurements made by high-sensitivity gages.

17. Key Words (Suggested by Author(s))	18. Distribution Statement
adhesive joints, thick adherend lap joint, cracked lap shear specimen moire interferometry, experimental analysis, displacement fields, strains	Unclassified-Unlimited Subject Category 27

19. Security Classif. (of this report)	20. Security Classif. (of this page)	21. No. of Pages	22. Price
Unclassifed	Unclassified	43	A03

For sale by the National Technical Information Service, Springfield, Virginia 22161